

WIND-TUNNEL STUDY OF WIND FLOW
OVER BDM BUILDING, ALBUQUERQUE

by

J. A. Peterka* and J. E. Cermak**

for

BDM Corporation
1801 Randolph Road, S.E.
Albuquerque, New Mexico 87106

Fluid Mechanics and Wind Engineering Program
Fluid Dynamics and Diffusion Laboratory
Department of Civil Engineering
Colorado State University
Fort Collins, Colorado 80523

CSU Project 2-95150

August 1982

*Associate Professor
**Professor-in-Charge, Fluid Mechanics and
Wind Engineering Program

TABLE OF CONTENTS

<u>Chapter</u>		<u>Page</u>
	LIST OF FIGURES	ii
	LIST OF SYMBOLS	iii
1	INTRODUCTION	1
	1.1 General	1
	1.2 The Wind-Tunnel Test	2
2	EXPERIMENTAL CONFIGURATION	3
	2.1 Wind Tunnel	3
	2.2 Model	3
3	INSTRUMENTATION AND DATA ACQUISITION	5
	3.1 Flow Visualization	5
	3.2 Velocity	5
4	RESULTS	7
	4.1 Flow Visualization	7
	4.2 Velocity	7
5	DISCUSSION	8
	5.1 Flow Visualization	8
	5.2 Velocity and Turbulence Profiles	8
	REFERENCES	10
	FIGURES	11
	FLOW VISUALIZATION GUIDE	46

LIST OF FIGURES

<u>Figure</u>		<u>Page</u>
1	Fluid Dynamics and Diffusion Laboratory	12
2	Wind-Tunnel Configuration	13
3	Model Installed in the Wind Tunnel	14
4	Flow Visualization	15
5	Mean Velocity and Turbulence Profiles Approaching the Model	29
6	Mean Velocity and Turbulence Profiles at Measuring Positions	30

LIST OF SYMBOLS

<u>Symbol</u>	<u>Definition</u>
U	Local mean velocity
D	Characteristic dimension (building height, width, etc.)
ν, ρ	Kinematic viscosity and density of approach flow
$\frac{UD}{\nu}$	Reynolds number
E	Mean voltage
A, B, n	Constants
U_{rms}	Root-mean-square of fluctuating velocity
E_{rms}	Root-mean-square of fluctuating voltage
U_{∞}	Reference mean velocity outside the boundary layer
Z	Height above surface
δ	Height of boundary layer
T_u	Turbulence intensity $\frac{U_{rms}}{U_{\infty}}$ or $\frac{U_{rms}}{U}$

1. INTRODUCTION

1.1 General

Solar collectors located on building tops may be exposed to winds amplified in speed by the presence of the building. The building geometry may increase or decrease wind loading on roof-mounted structures. Wind forces may be modified by nearby structures which can produce beneficial shielding or adverse increases in loading. Overestimating loads results in uneconomical design; underestimating may result in structural failures.

Techniques have been developed for wind-tunnel modeling of proposed structures which allow the prediction of wind pressures on cladding and windows, overall structural loading, loading on roof-mounted structures, and also wind velocities and gusts in pedestrian areas adjacent to the building.

Modeling of the aerodynamic loading on a structure requires special consideration of flow conditions in order to guarantee similitude between model and prototype. A detailed discussion of the similarity requirements and their wind-tunnel implementation can be found in references (1), (2), and (3). In general, the requirements are that the model and prototype be geometrically similar, that the approach mean velocity at the building site have a vertical profile shape similar to the full-scale flow, that the turbulence characteristics of the flows be similar, and that the Reynolds number for the model and prototype be equal.

These criteria are satisfied by constructing a scale model of the structure and its surroundings and performing the wind tests in a wind tunnel specifically designed to model atmospheric boundary-layer flows. Reynolds number similarity requires that the quantity UD/ν be similar

for model and prototype. Since ν , the kinematic viscosity of air, is identical for both, Reynolds numbers cannot be made precisely equal with reasonable wind velocities. To accomplish this the air velocity in the wind tunnel would have to be as large as the model scale factor times the prototype wind velocity, a velocity which would introduce unacceptable compressibility effects. However, for sufficiently high Reynolds numbers ($>2 \times 10^4$) the pressure coefficient at any location on the structure will be essentially constant for a large range of Reynolds numbers. Typical values encountered are 10^7 - 10^8 for the full-scale and 10^5 - 10^6 for the wind-tunnel model. In this range acceptable flow similarity is achieved without precise Reynolds number equality.

1.2 The Wind-Tunnel Test

The wind-engineering study is performed on a building or building group modeled at scales ranging from 1:150 to 1:400. The building model is constructed of clear plastic fastened together with screws. The structure is modeled in detail to provide accurate flow patterns in the wind passing over the building surfaces. The building under test is often located in a surrounding where nearby buildings or terrain may provide beneficial shielding or adverse wind loading. To achieve similarity in wind effects the area surrounding the test building is also modeled. For this study no additional buildings were modeled. A flow visualization study is first made (smoke is used to make the air currents visible) to define overall flow patterns and identify regions where local flow features might cause difficulties.

The following pages discuss in greater detail the procedures followed and the equipment and data collecting and processing methods used. In addition, the data presentation format is explained and the implications of the data are discussed.

2. EXPERIMENTAL CONFIGURATION

2.1 Wind Tunnel

Wind-engineering studies are performed in the Fluid Dynamics and Diffusion Laboratory at Colorado State University (Figure 1). Three large wind tunnels are available for wind loading studies depending on the detailed requirements of the study. The wind tunnel used for this investigation is shown in Figure 2. All tunnels have a flexible roof adjustable in height to maintain a zero pressure gradient along the test section. The mean velocity can be adjusted continuously in each tunnel to the maximum velocity available.

2.2 Model

In order to obtain an accurate assessment of the local wind environment, models are constructed to the largest scale that does not produce significant blockage in the wind-tunnel test section. The models are constructed of 1/2 in. thick Lucite plastic and fastened together with metal screws.

A circular area 750 to 2000 ft in radius depending on model scale and characteristics of the surrounding buildings and terrain is modeled in detail. Structures within the modeled region are made from styrofoam and cut to the individual building geometries. They are mounted on the turntable in their proper locations. Significant terrain features are included as needed. The model is mounted on a turntable (Figure 2) near the downwind end of the test section. Any buildings or terrain features which do not fit on the turntable are placed on removable pieces which are placed upwind of the turntable for appropriate wind directions. Because no structures of significance to the study were located nearby, no additional structures were modeled. A plan view of the building and

its surroundings is shown in Figure 3. The turntable is calibrated to indicate azimuthal orientation to 0.1 degree.

The region upstream from the modeled area is covered with a randomized roughness constructed using various sized cubes placed on the floor of the wind tunnel. Different roughness sizes may be used for different wind directions. Spires are installed at the test-section entrance to provide a thicker boundary layer than would otherwise be available. The thicker boundary layer permits a somewhat larger scale model than would otherwise be possible. The spires are approximately triangularly shaped pieces of 1/2 in.-thick plywood 6 in. wide at the base and 1 in. wide at the top, extending from the floor to the top of the test section. They are placed so that the broad side intercepts the flow. A barrier approximately 8 in. high is placed on the test-section floor downstream of the spires to aid in development of the boundary-layer flow.

The distribution of the roughness cubes and the spires in the roughened area were designed to provide a boundary-layer thickness of approximately 4 ft, a velocity profile power-law exponent similar to that expected to occur in the region approaching the modeled area for each wind direction (a number of wind directions may have the same approach roughness). Photographs of the model in the wind tunnel are shown in Figures 3 and 4. The wind-tunnel ceiling is adjusted after placement of the model to obtain a zero pressure gradient along the test section.

3. INSTRUMENTATION AND DATA ACQUISITION

3.1 Flow Visualization

Making the air flow visible in the vicinity of the model is helpful in defining zones of separated flow and reattachment and zones of vortex formation where loads of roof-mounted collectors may be expected to be high. Titanium tetrachloride smoke is released from sources on and near the model to make the flow lines visible to the eye and to make it possible to obtain motion picture records of the tests. Conclusions obtained from these smoke studies are discussed in Sections 4.1 and 5.1.

3.2 Velocity

Mean velocity and turbulence intensity profiles are measured upstream of the model to determine that an approach boundary-layer flow appropriate to the site has been established. Tests are made at one wind velocity in the tunnel. This velocity is well above that required to produce Reynolds number similarity between the model and the prototype as discussed in Section 1.1.

In addition, mean velocity and turbulence intensity profiles are made on or near the building at several locations for various wind directions. The measurement locations are shown on Figure 3. These measurements indicate the magnitude and location of accelerated flow over the building roof.

Measurements are made with a single hot-wire anemometer mounted with its axis vertical. The instrumentation used is a Thermo Systems constant temperature anemometer (Model 1050) with a 0.001-in. diameter platinum film sensing element 0.020 in. long. Output is directed to the on-line data acquisition system for analysis.

Calibration of the hot-wire anemometer is performed by comparing output with the pitot-static tube in the wind tunnel. The calibration data are fit to a variable exponent King's Law relationship of the form

$$E^2 = A + BU^n$$

where E is the hot-wire output voltage, U the velocity and A , B , and n are coefficients selected to fit the data. The above relationship was used to determine the mean velocity at measurement points using the measured mean voltage. The fluctuating velocity in the form U_{rms} (root-mean-square velocity) was obtained from

$$U_{\text{rms}} = \frac{2 E E_{\text{rms}}}{B n U^{n-1}}$$

where E_{rms} is the root-mean-square voltage output from the anemometer. Turbulence intensity in velocity profile measurements used the local mean velocity.

4. RESULTS

4.1 Flow Visualization

A film is included as part of this report showing the characteristics of flow about the structure using smoke to make the flow visible. A listing of the contents of the film is shown in Table 1. Several features can be noted from the visualization. A description of the smoke test results emphasizing flow patterns of concern relative to possible high-wind load areas and pedestrian comfort is given in Section 5.1.

4.2 Velocity

Velocity and turbulence profiles are shown in Figure 5. Profiles were taken upstream from the model which are characteristic of the boundary layer approaching the model and at various locations above the building roof, as shown in Figure 3. The boundary-layer thickness, δ , is shown in Figure 5. The corresponding prototype value of δ for this study is also shown in the figure. This value was established as a reasonable height for this study. The mean velocity profile approaching the modeled area has the form

$$\frac{U}{U_{\infty}} = \left(\frac{z}{\delta}\right)^n .$$

The exponent n for the approach flow established for this study is shown in Figure 5.

Profiles of longitudinal turbulence intensity in the flow approaching the modeled area are shown in Figure 5. The turbulence intensities are appropriate for the approach mean velocity profile selected. For the velocity profiles, turbulence intensity is defined as the root-mean-square about the mean of the longitudinal velocity fluctuations divided by the local mean velocity U ,

$$Tu = \frac{U_{rms}}{U} .$$

5. DISCUSSION

5.1 Flow Visualization

Flow patterns identified with smoke were observed for three parapet conditions: existing parapet, 8-ft 50 percent porosity parapet, and 8-ft solid parapet. In all cases, flow over the top of the building was observed to separate from the surface forming a pocket of low velocity air (the separated zone) immediately over the roof. For the existing parapet, the separated zone was insufficient in height to prevent high-velocity wind at the edge of the separated zone from hitting the collector closest to the edge of the building. The 8-ft solid parapet caused the separated zone to extend above the collectors for most wind directions effectively removing the high winds from the collectors. The 50 percent porous screen appeared to lower the velocities hitting the lead collector and made the edge of the separated zone more difficult to detect.

For all cases, a pair of rooftop vortices was observed to originate from the upwind corner for winds approaching from 45 degrees to the building face. Vortices of this type are known to bring higher velocity fluid down closer to the roof.

5.2 Velocity and Turbulence Profiles

Figure 3 shows the four locations selected for study. Data was taken with the existing parapet in place, with an 8-ft high parapet with 50 percent porosity in place, and with an 8-ft high solid parapet in place. Data for each of these configurations was taken at wind directions 45, 90, 135 and 270. All of the profiles were taken with the solar collectors removed. Profiles are shown in Figure 6 in comparison to the approach wind profile. Photographs corresponding to these profiles are shown in Figure 4.

In general, wind velocities decreased as the parapet porosity decreased. Note that wind load varies with the square of wind velocity. The only exception to the generality that decreased porosity in the parapet created decreased velocity occurred for position 2 at wind directions perpendicular to the structure (azimuths 90 and 270). In these cases, wind flow over the solid parapet reattached to the inner portion of the roof. The increase in velocity for these cases was slight, however, compared to the reductions in velocity obtained at other locations and wind directions by using a solid parapet. For example, at location 1 at wind direction 45, the mean velocity at the roof level was reduced from 40 percent of the boundary-layer speed to 15 percent by replacing the existing parapet with an 8-ft high solid parapet.

Unlike velocity, turbulence was found to increase (usually) as the porosity of the parapet decreased. Greater turbulence resulted from increased mixing induced by the parapets. Increased wind turbulence will increase somewhat dynamic loads on the collectors. This is more than compensated by a reduced mean load due to lower mean velocities.

The results of the study show that, overall, increasing the parapet porosity from 0 (as it exists today) toward 1 (a solid parapet) will reduce wind loads on the solar collectors on the roof.

REFERENCES

1. Cermak, J. E., "Laboratory Simulation of the Atmospheric Boundary Layer," AIAA Jl., Vol. 9, September 1971.
2. Cermak, J. E., "Applications of Fluid Mechanics to Wind Engineering," A Freeman Scholar Lecture, ASME Jl. of Fluids Engineering, Vol. 97, No. 1, March 1975.
3. Cermak, J. E., "Aerodynamics of Buildings," Annual Review of Fluid Mechanics, Vol. 8, 1976, pp. 75-106.

FIGURES

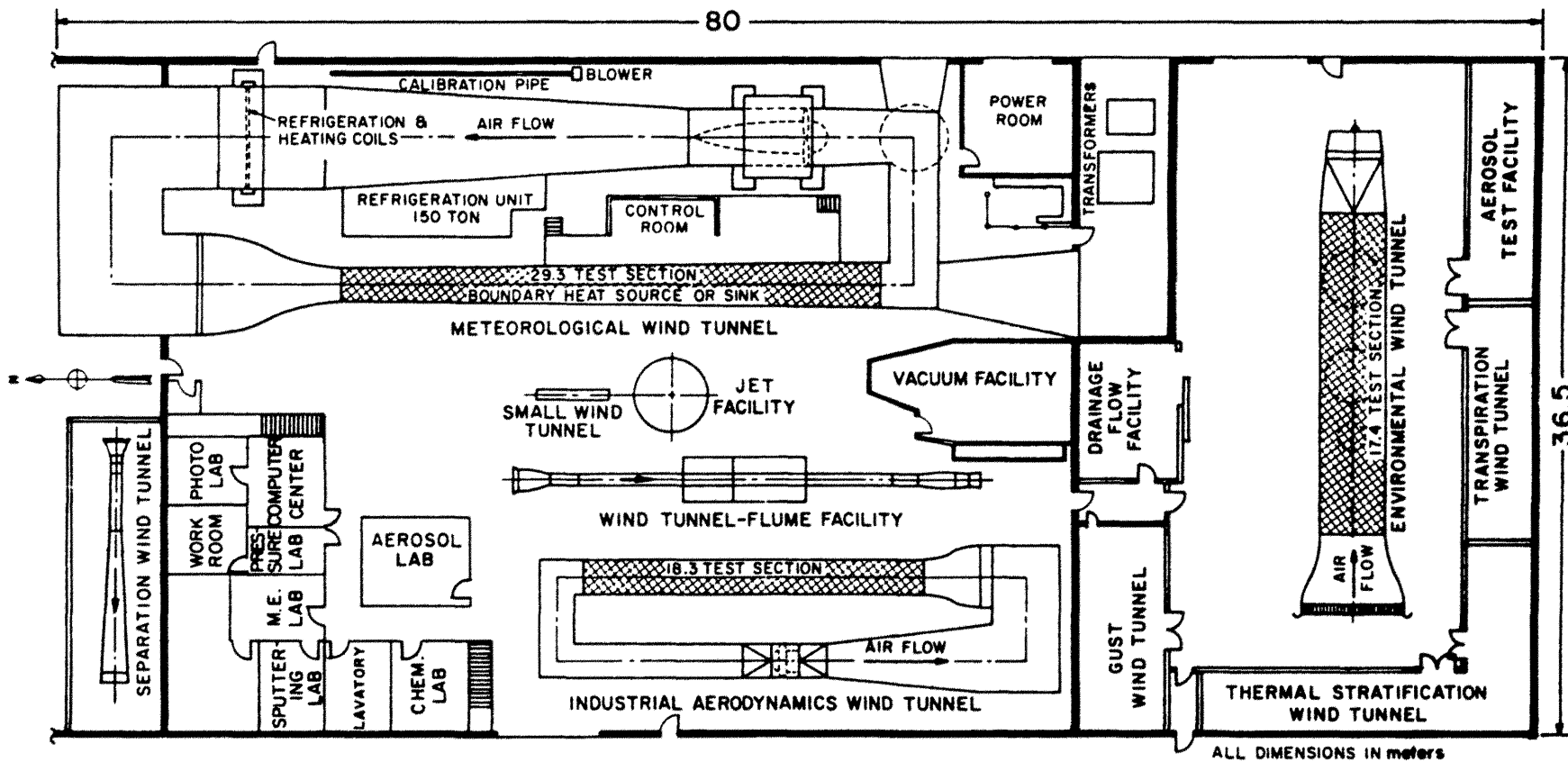
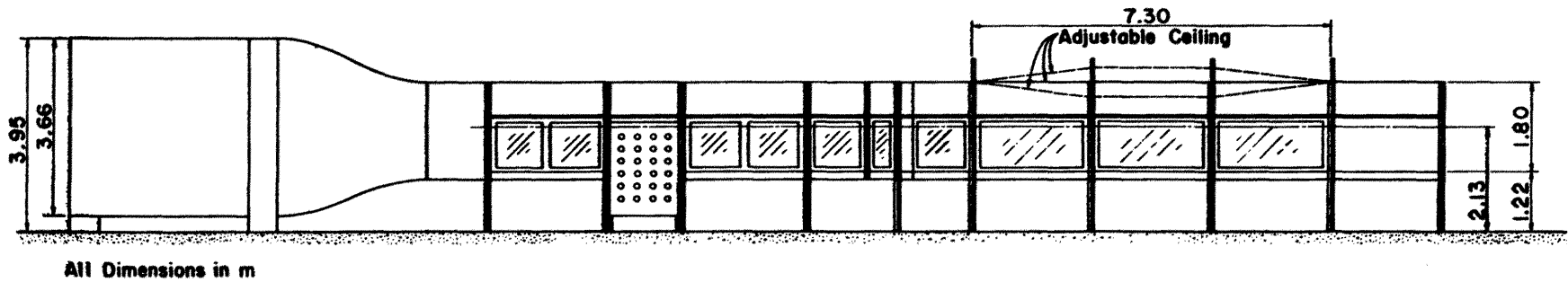
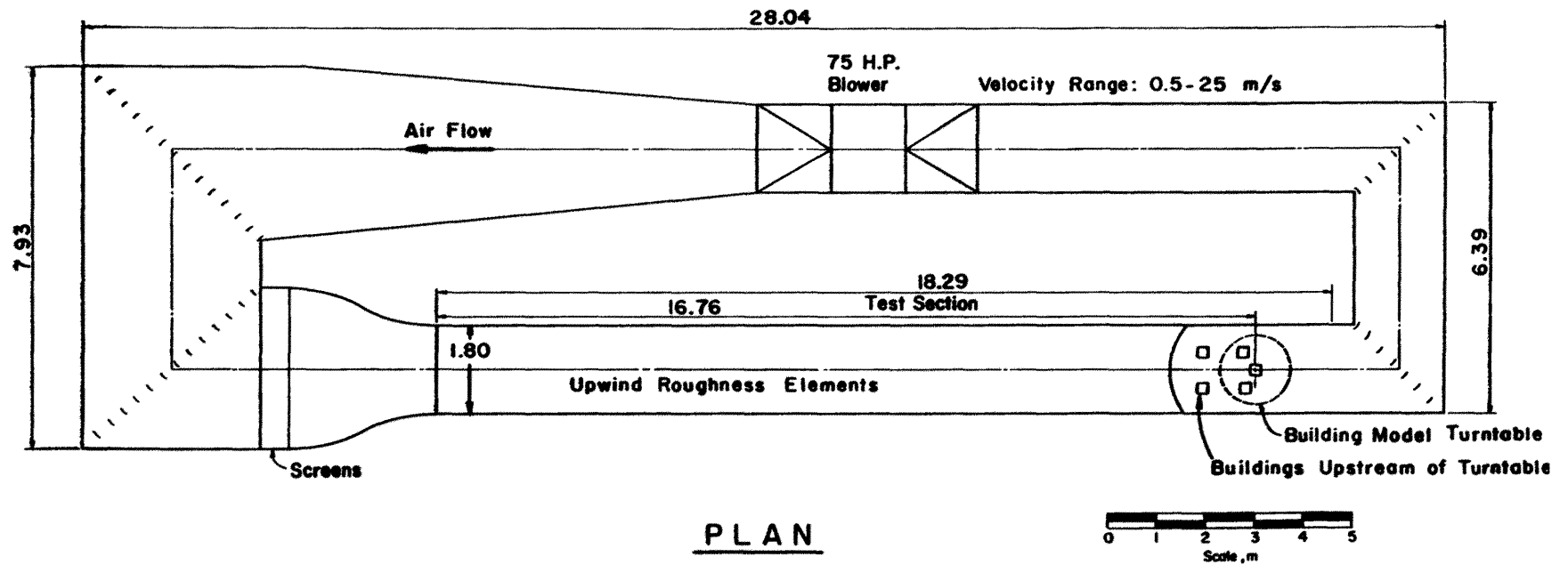


Figure 1. FLUID DYNAMICS AND DIFFUSION LABORATORY
COLORADO STATE UNIVERSITY



ELEVATION

INDUSTRIAL AERODYNAMICS WIND TUNNEL

Figure 2. Wind-Tunnel Configuration

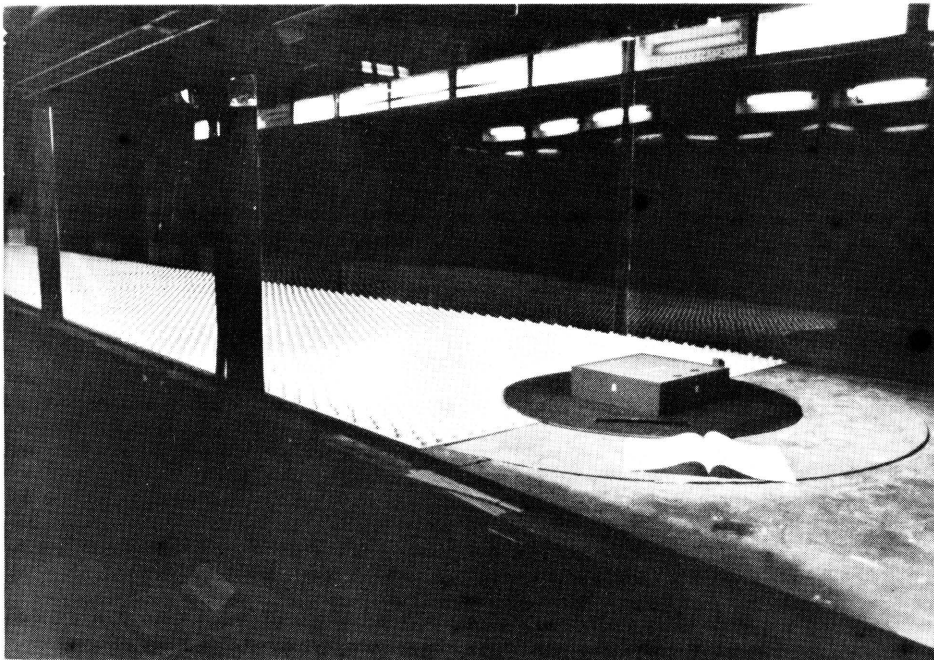
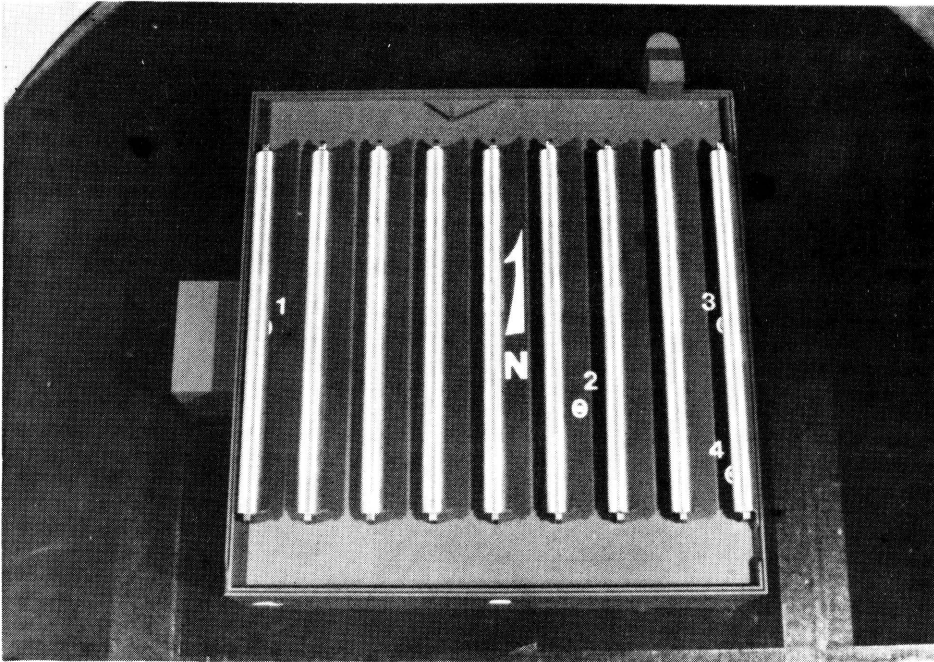


Figure 3. Model Installed in the Wind Tunnel

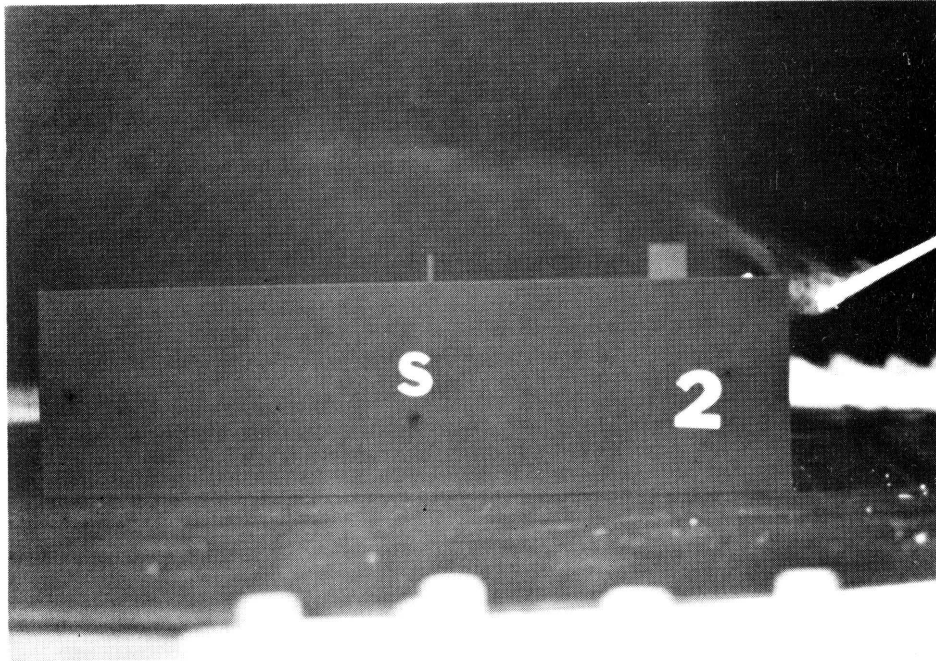
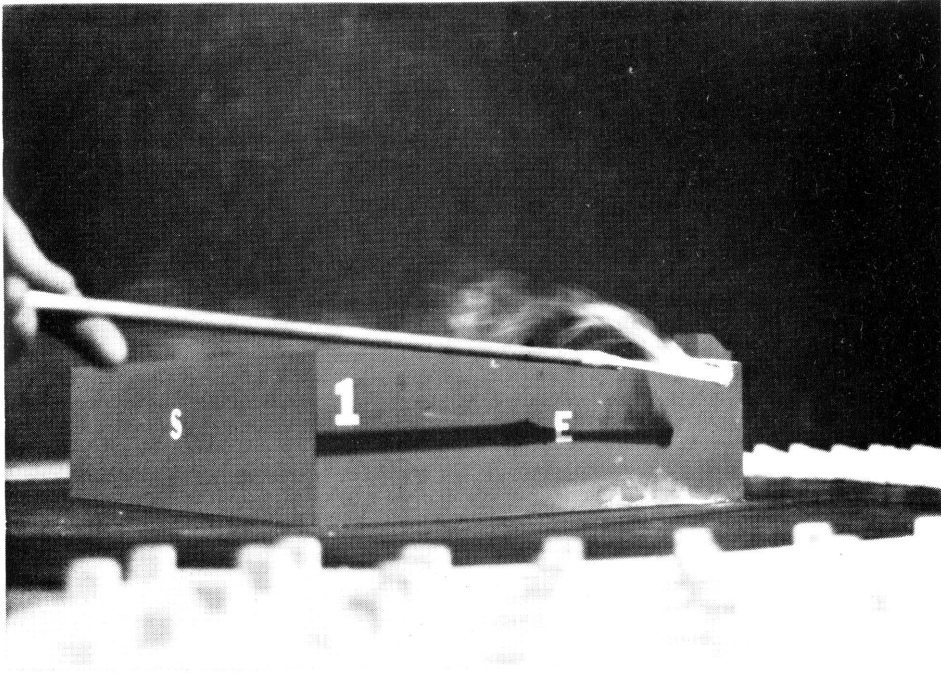


Figure 4a. Flow Visualization--Table 1 Gives Flow Conditions by Number

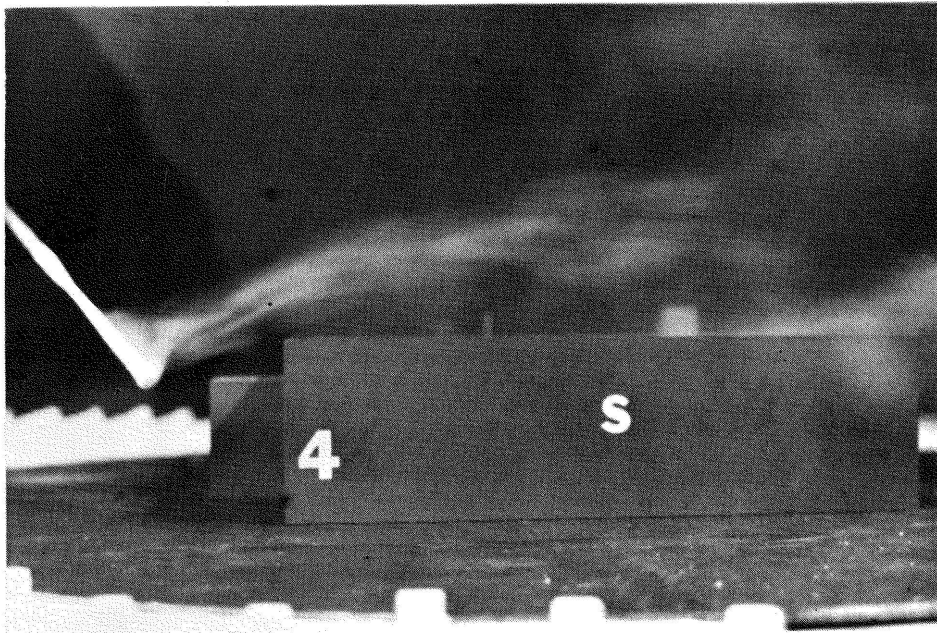
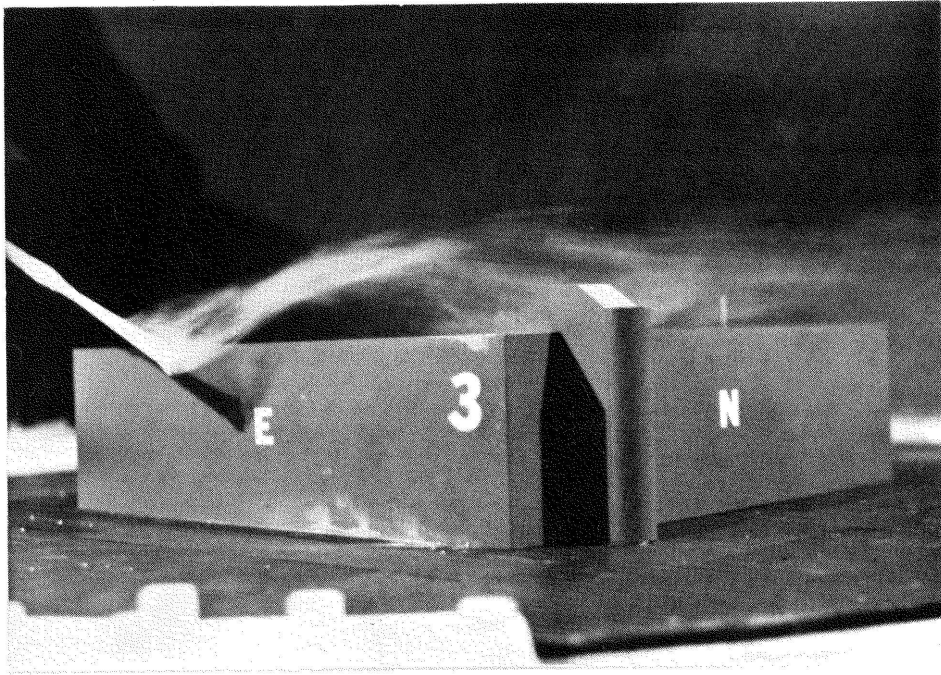


Figure 4b. Flow Visualization--Table 1 Gives Flow Conditions by Number

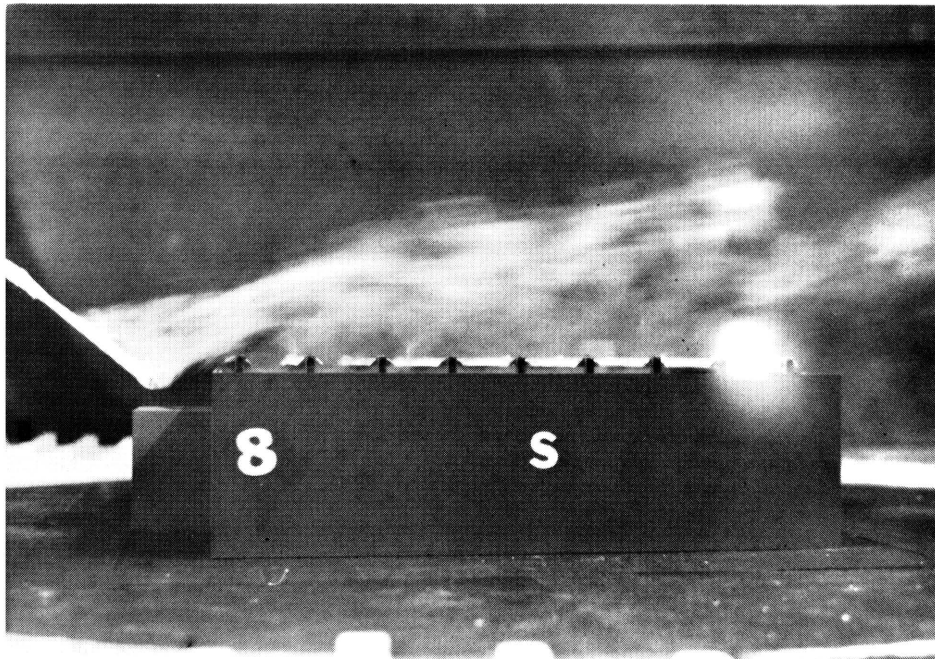
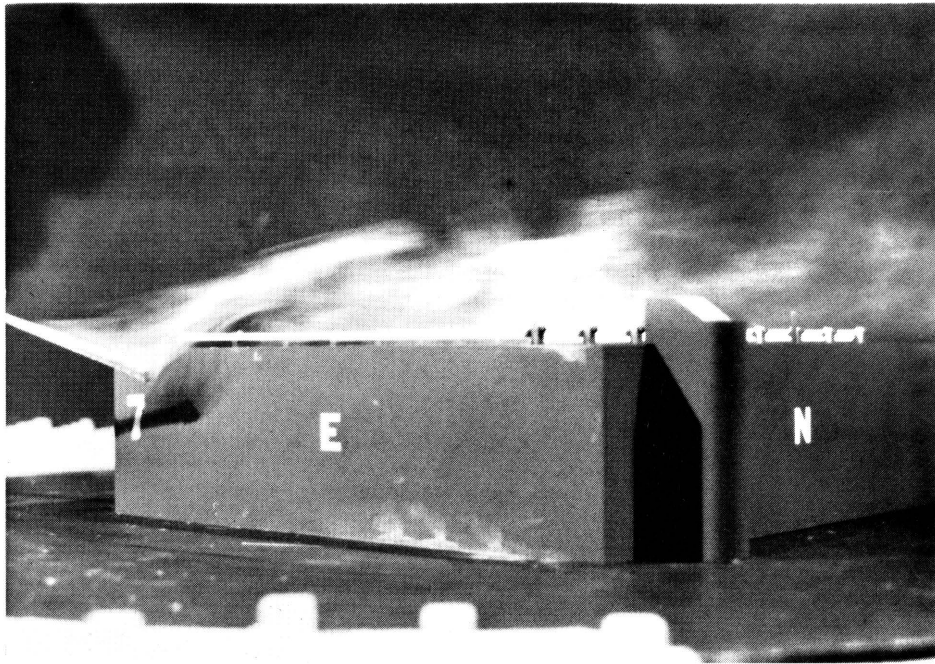


Figure 4c. Flow Visualization--Table 1 Gives Flow Conditions by Number

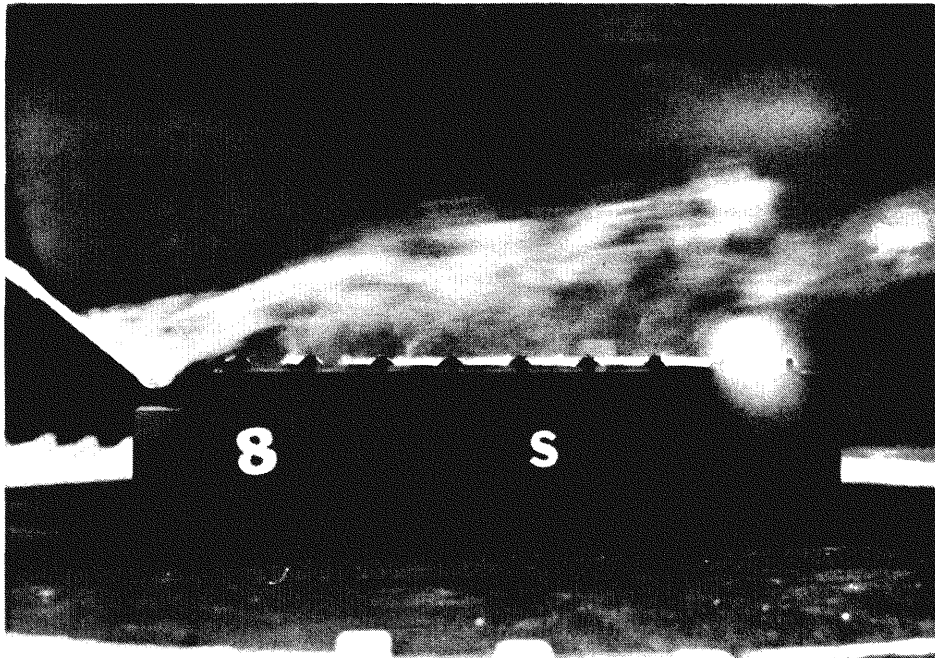
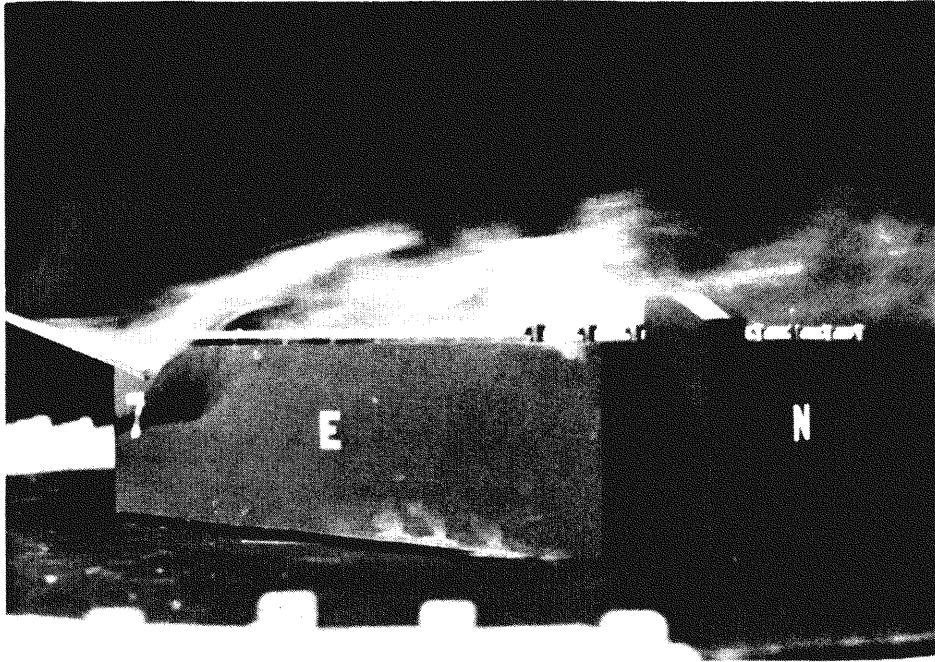


Figure 4d. Flow Visualization--Table 1 Gives Flow Conditions by Number

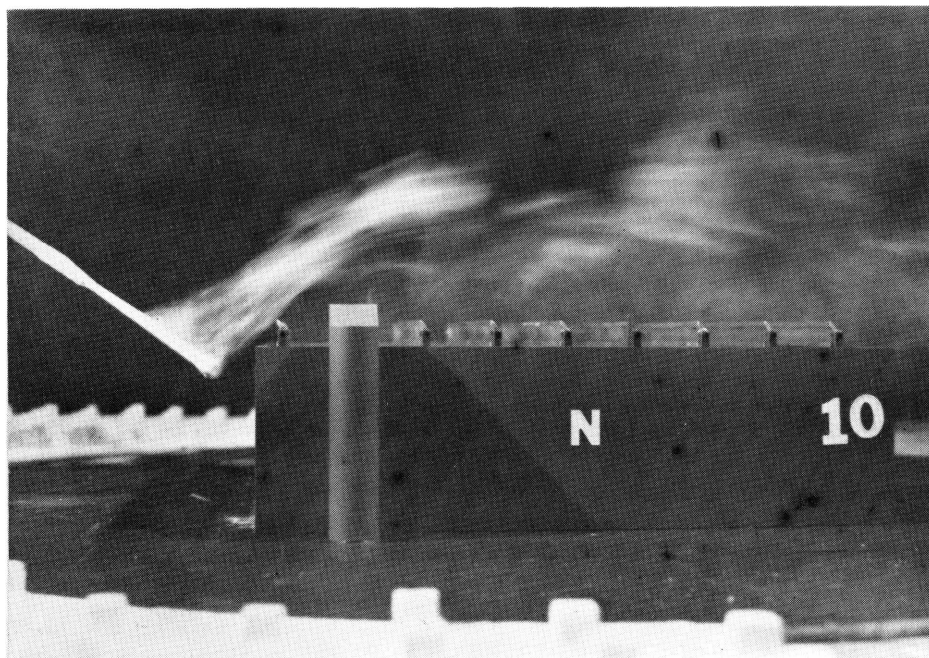
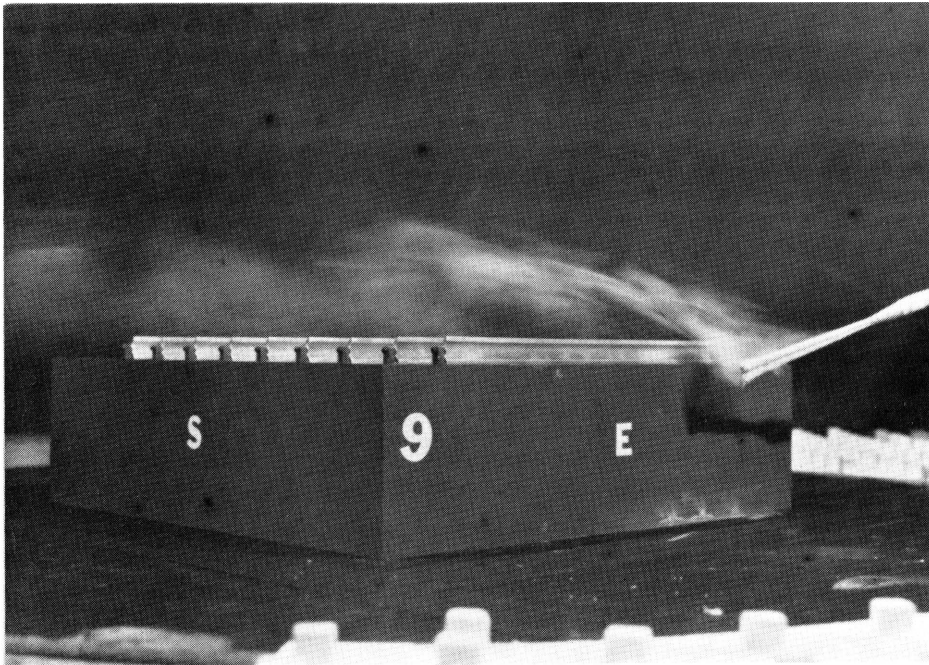


Figure 4e. Flow Visualization--Table 1 Gives Flow Conditions by Number

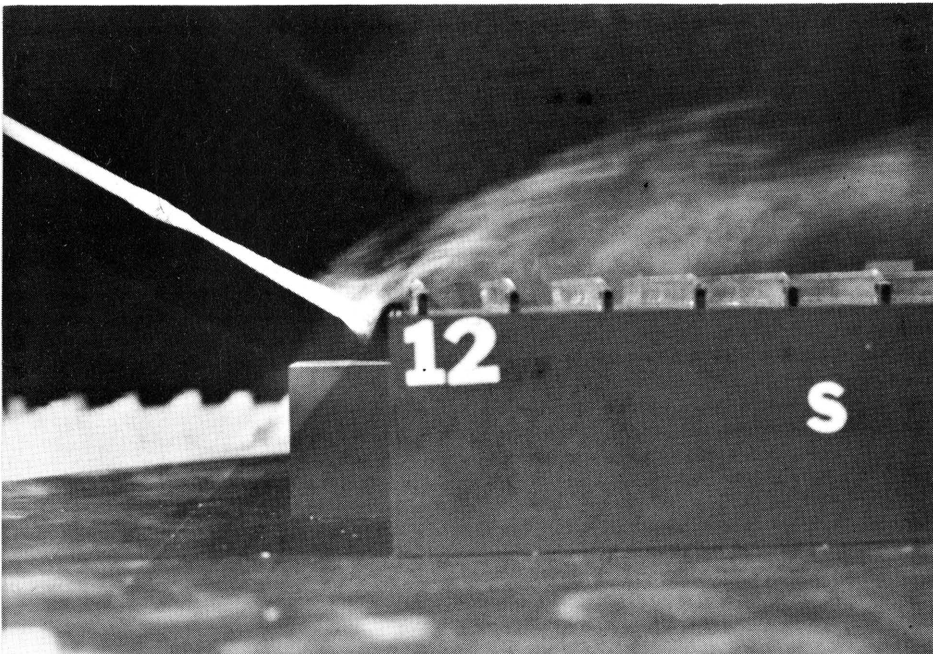
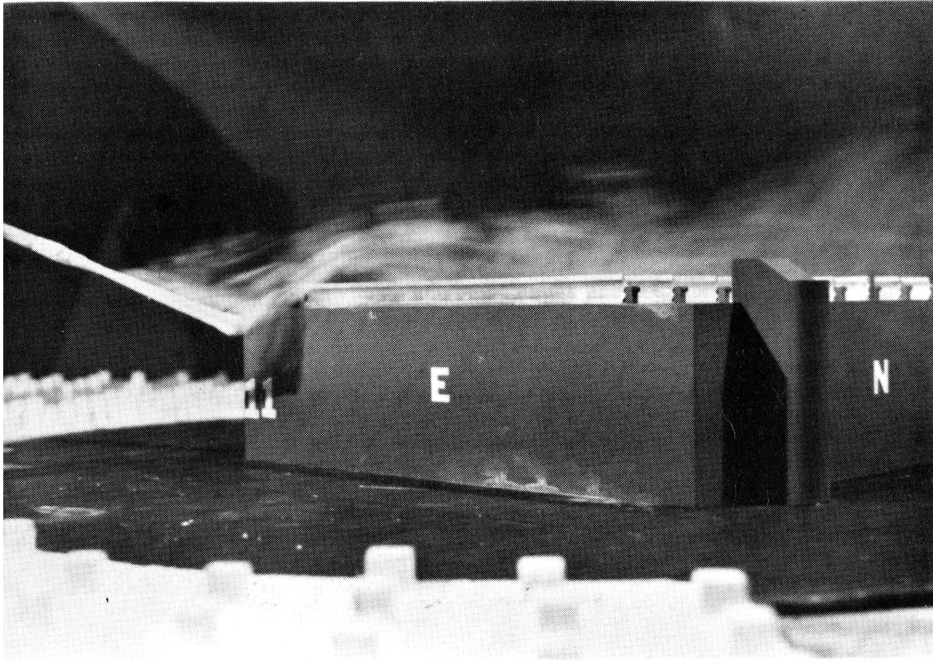


Figure 4f. Flow Visualization--Table 1 Gives Flow Conditions by Number

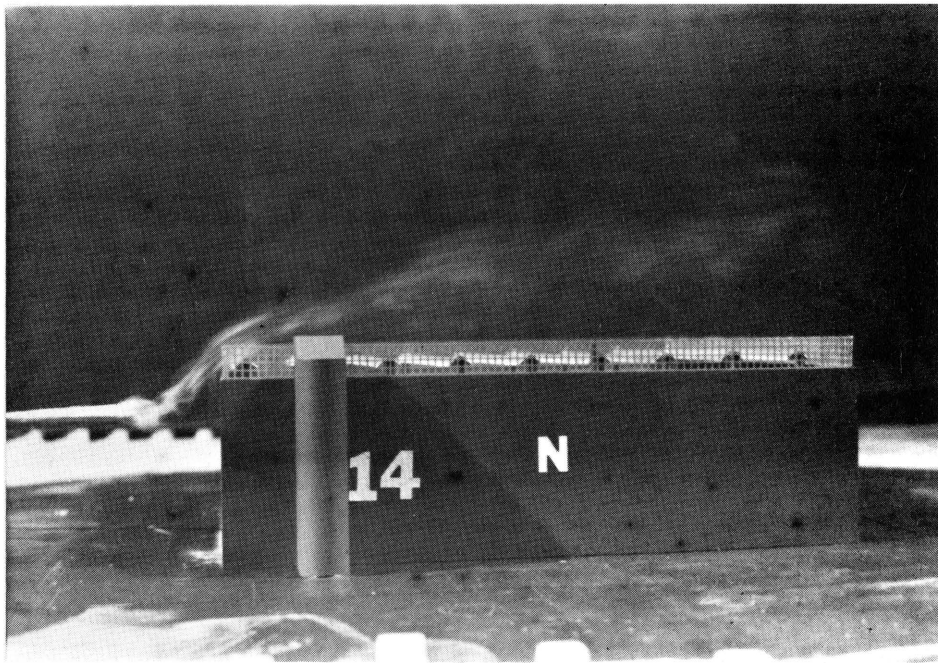
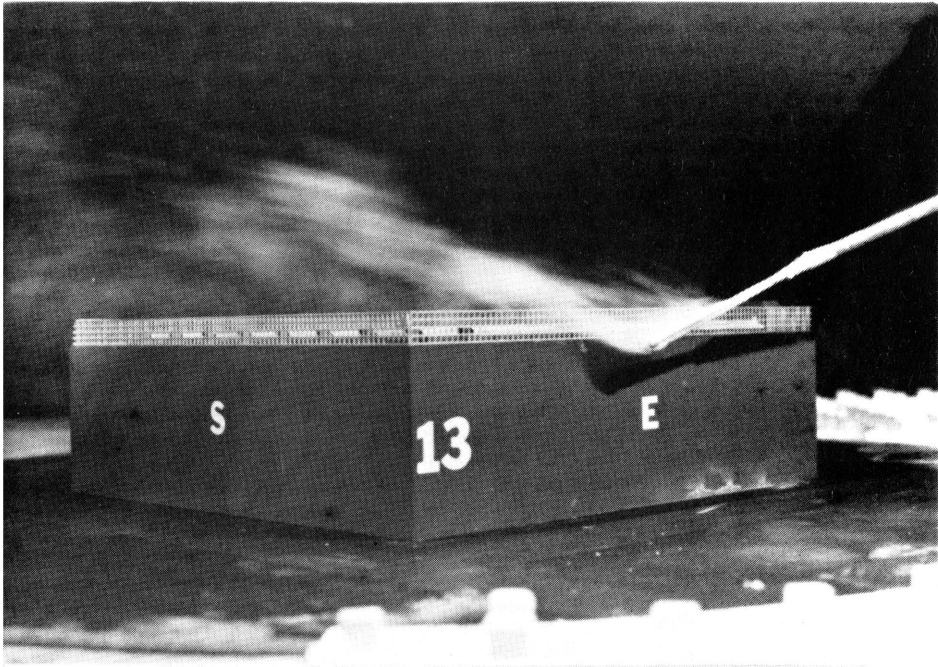


Figure 4g. Flow Visualization--Table 1 Gives Flow Conditions by Number

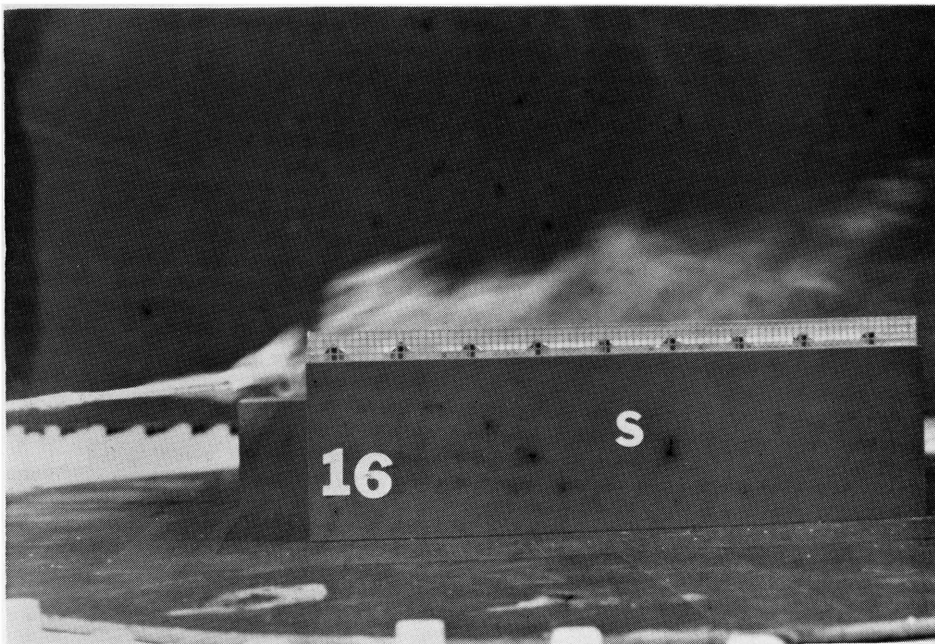
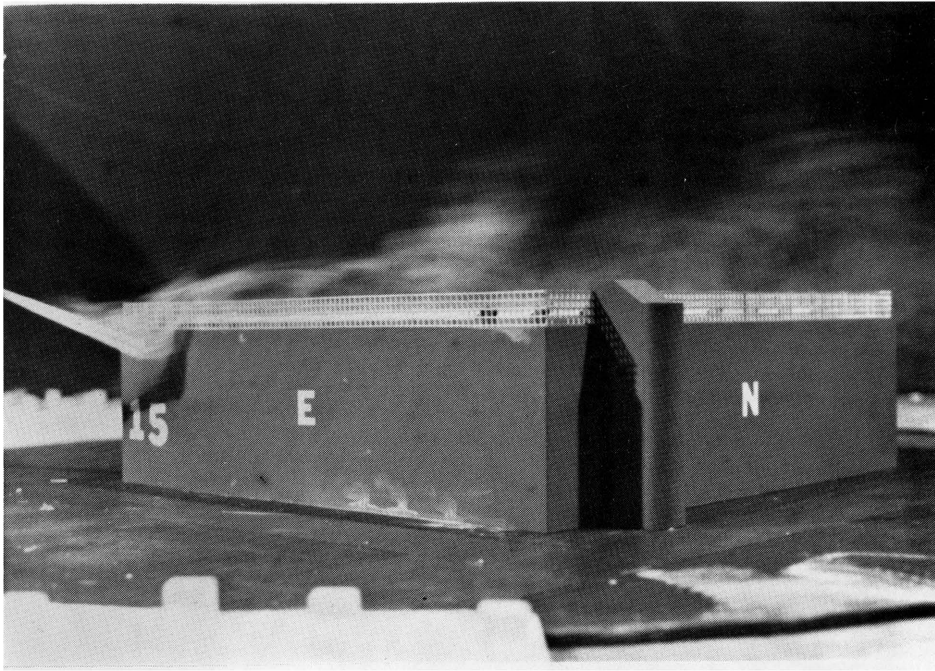


Figure 4h. Flow Visualization--Table 1 Gives Flow Conditions by Number

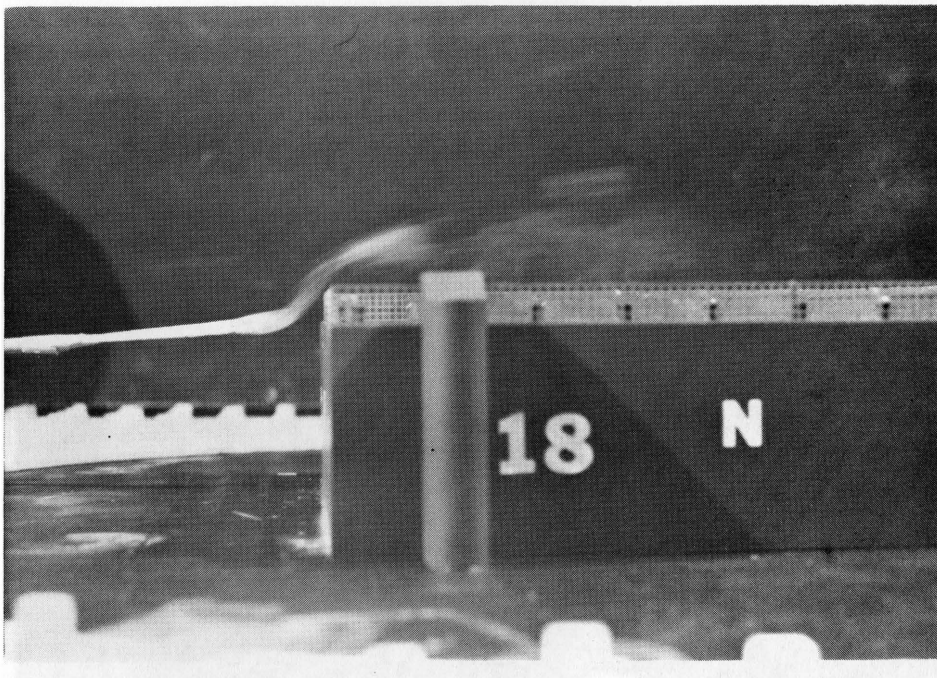
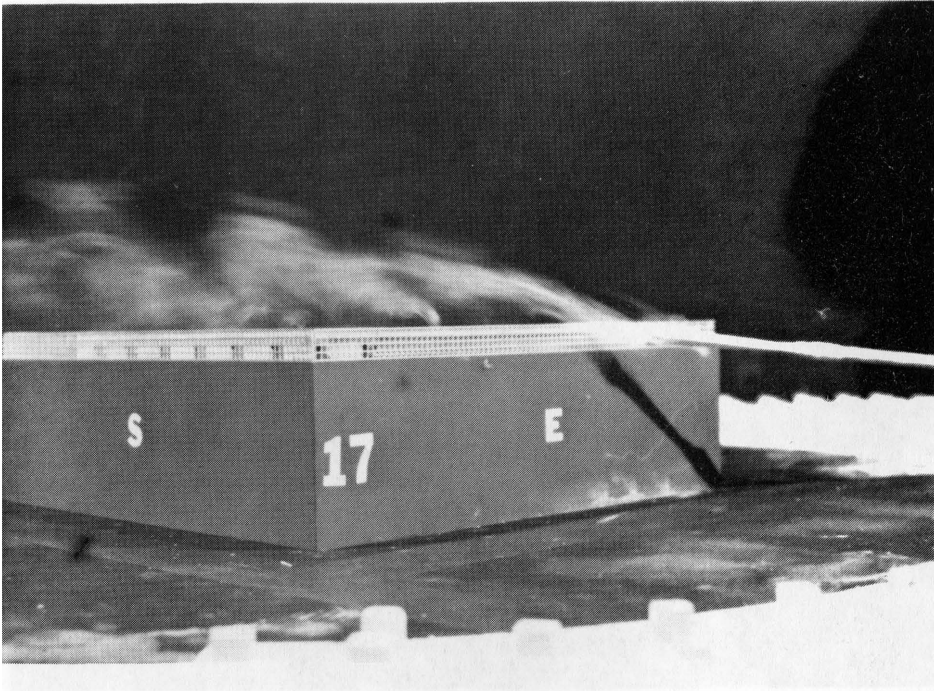


Figure 4i. Flow Visualization--Table 1 Gives Flow Conditions by Number

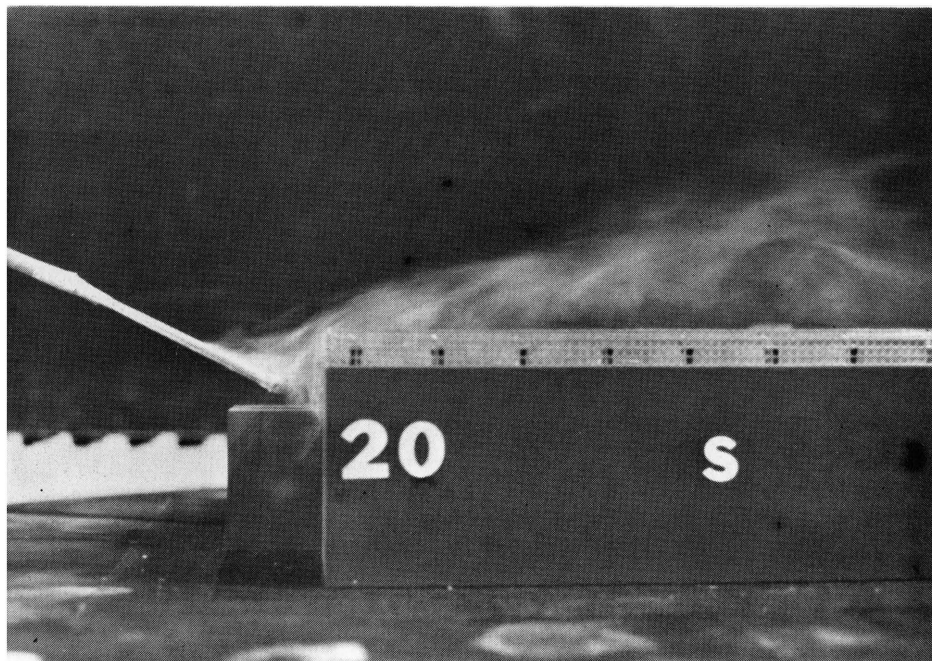
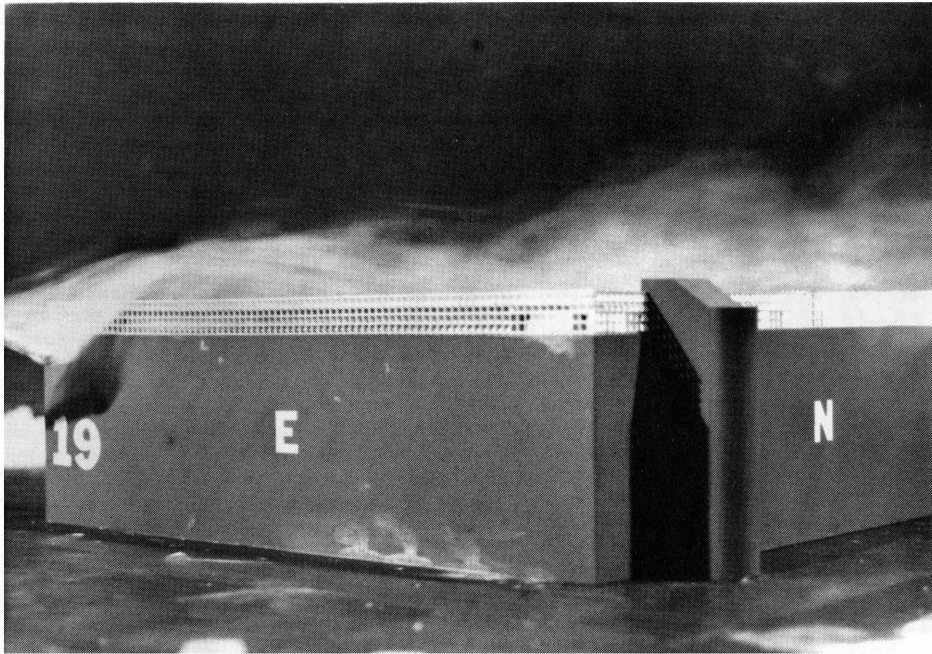


Figure 4j. Flow Visualization--Table 1 Gives Flow Conditions by Number

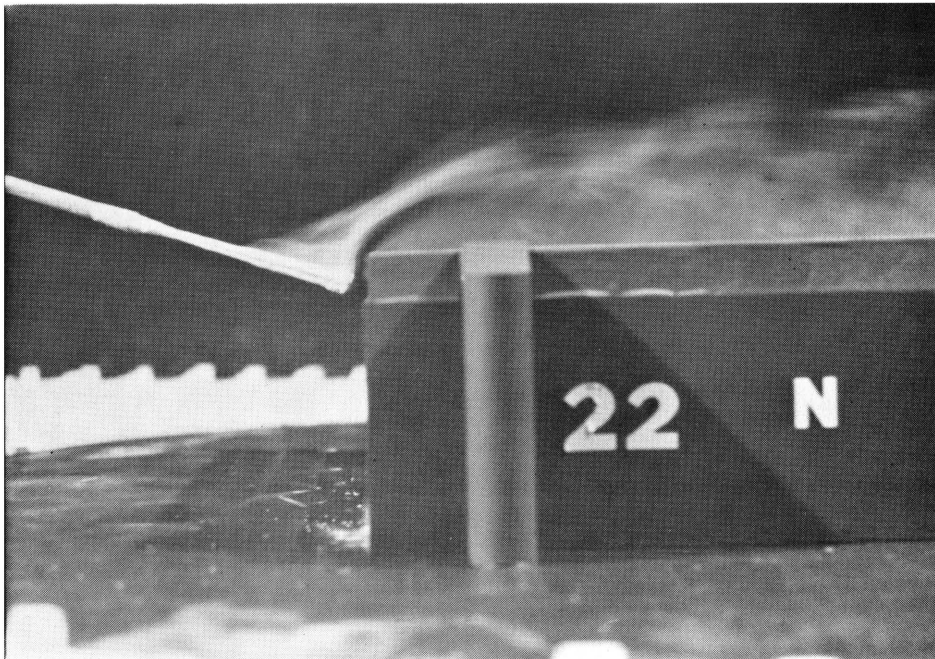
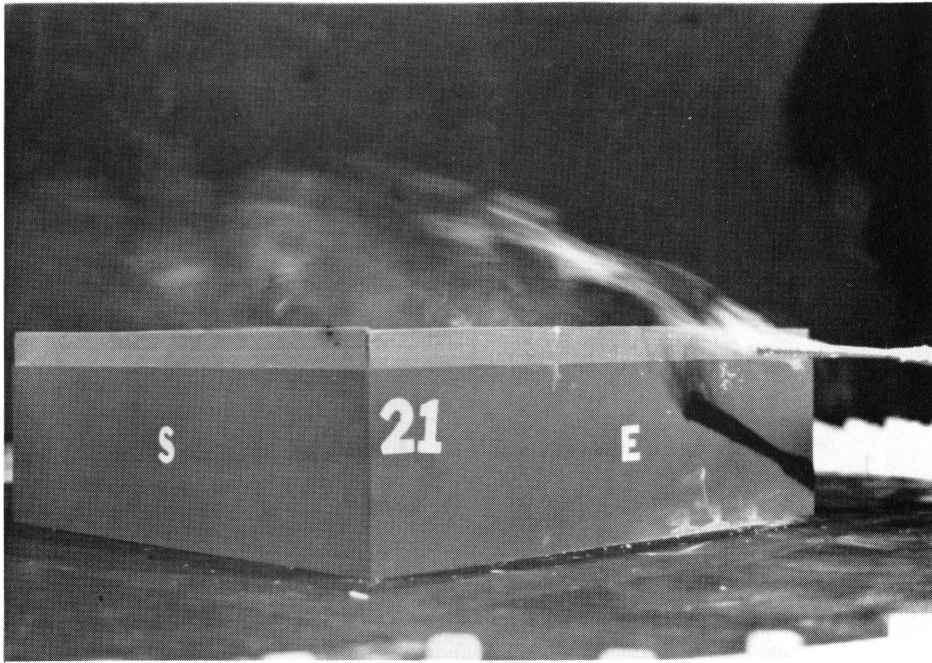


Figure 4k. Flow Visualization--Table 1 Gives Flow Conditions by Number

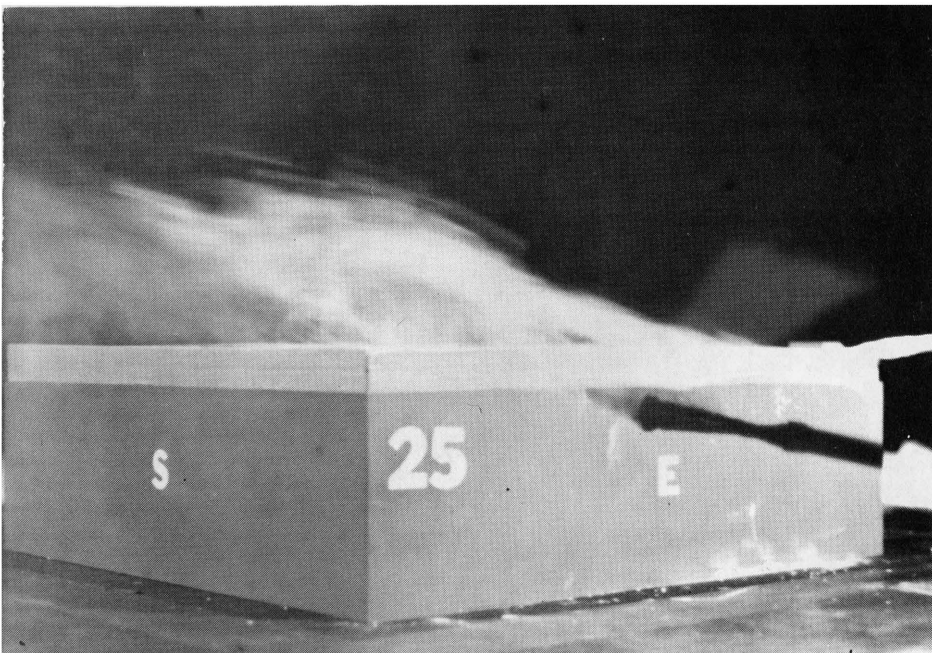
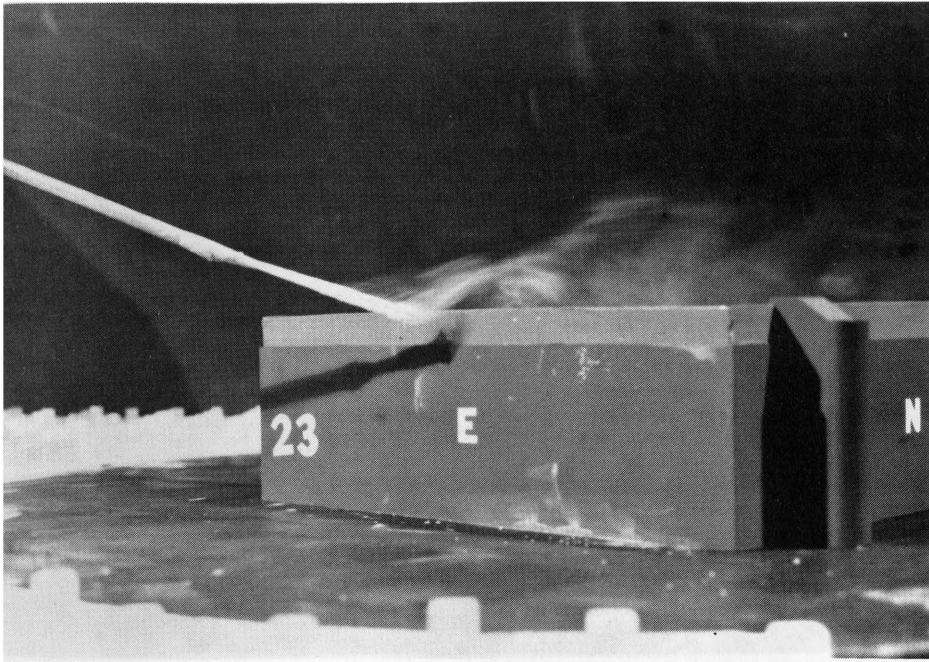


Figure 41. Flow Visualization--Table 1 Gives Flow Conditions by Number

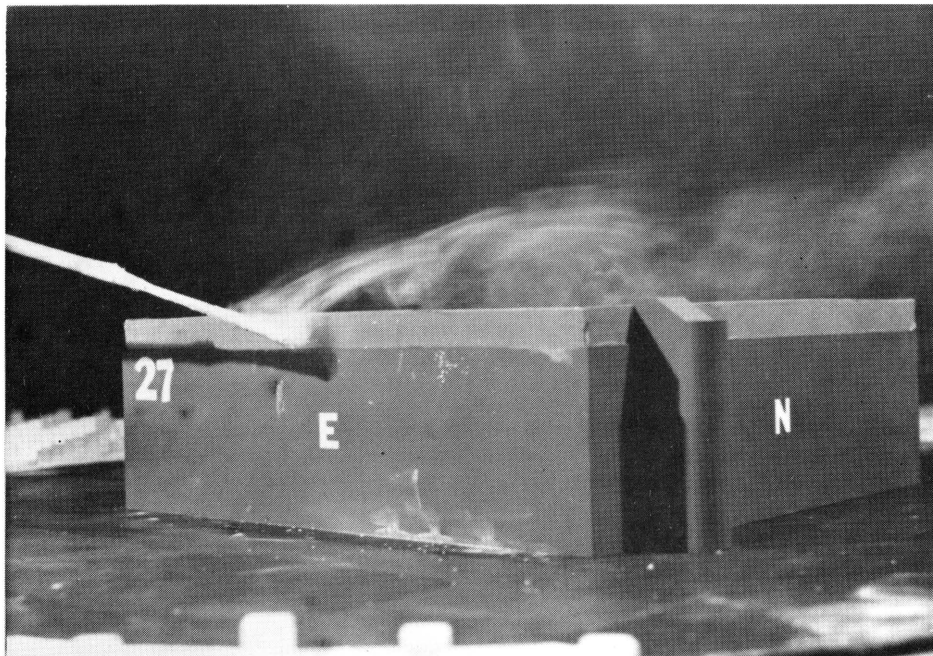
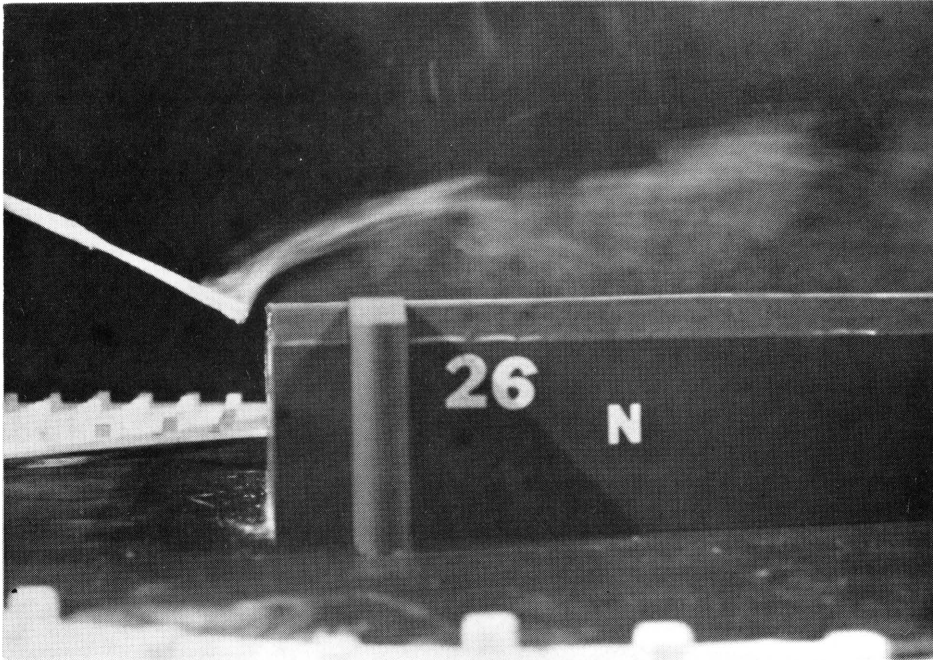


Figure 4m. Flow Visualization--Table 1 Gives Flow Conditions by Number

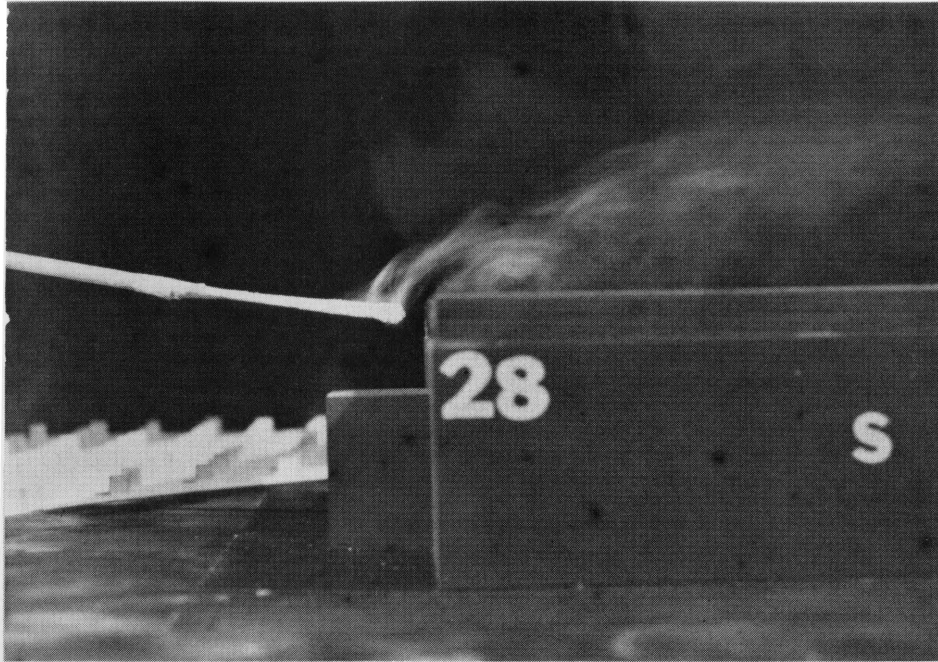


Figure 4n. Flow Visualization--Table 1 Gives Flow Conditions by Number

APPROACH

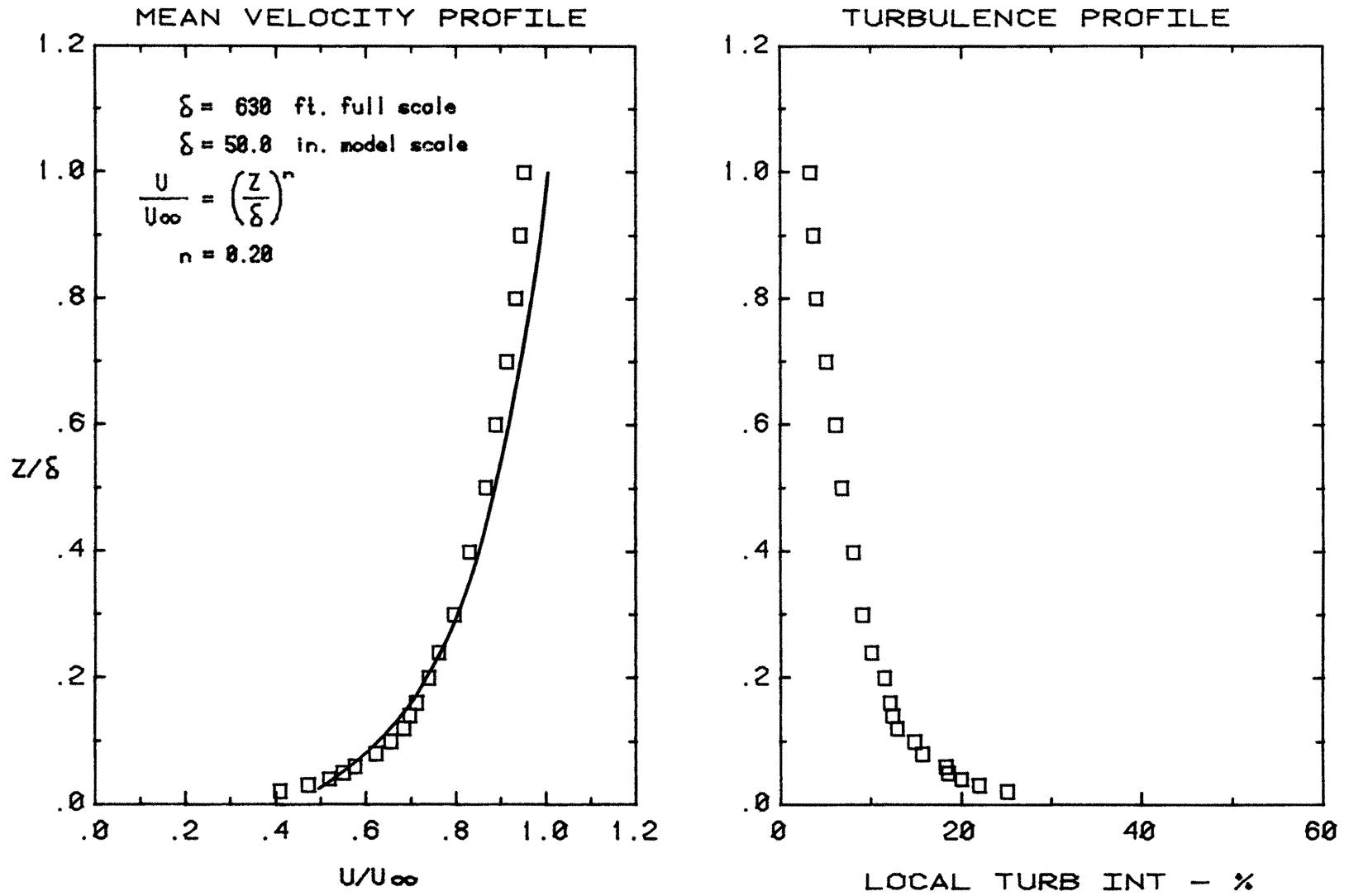


Figure 5. Mean Velocity and Turbulence Profiles Approaching the Model

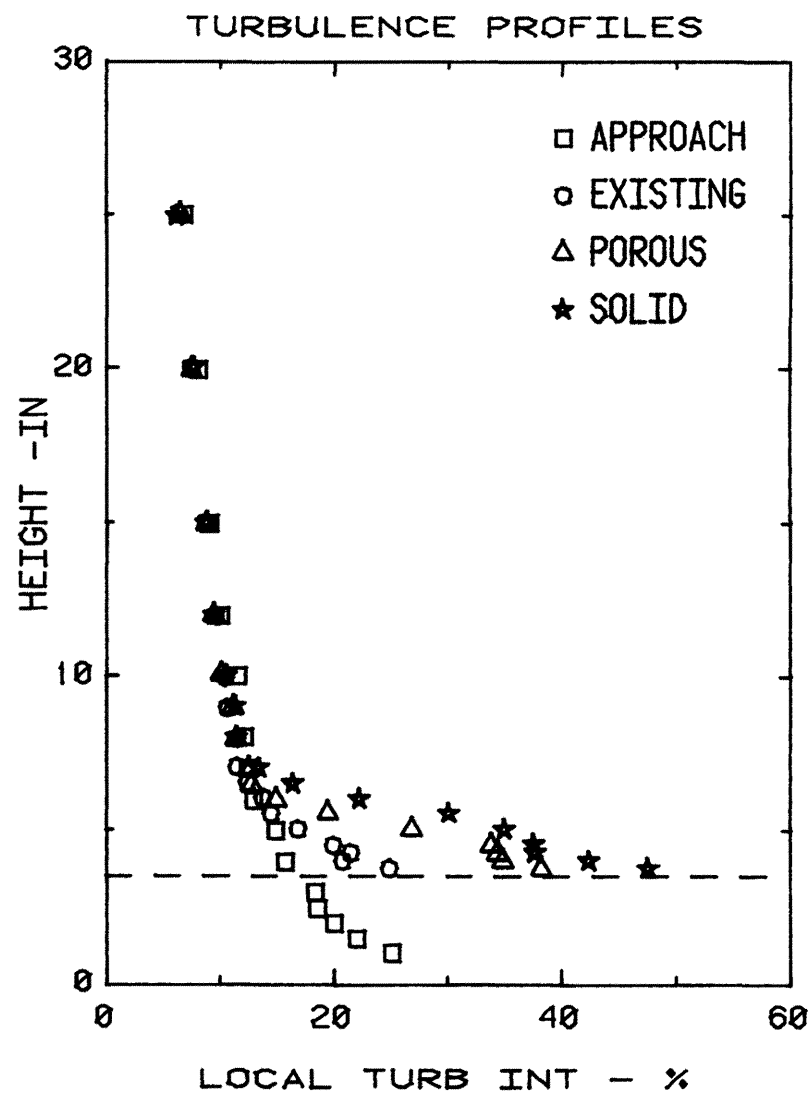
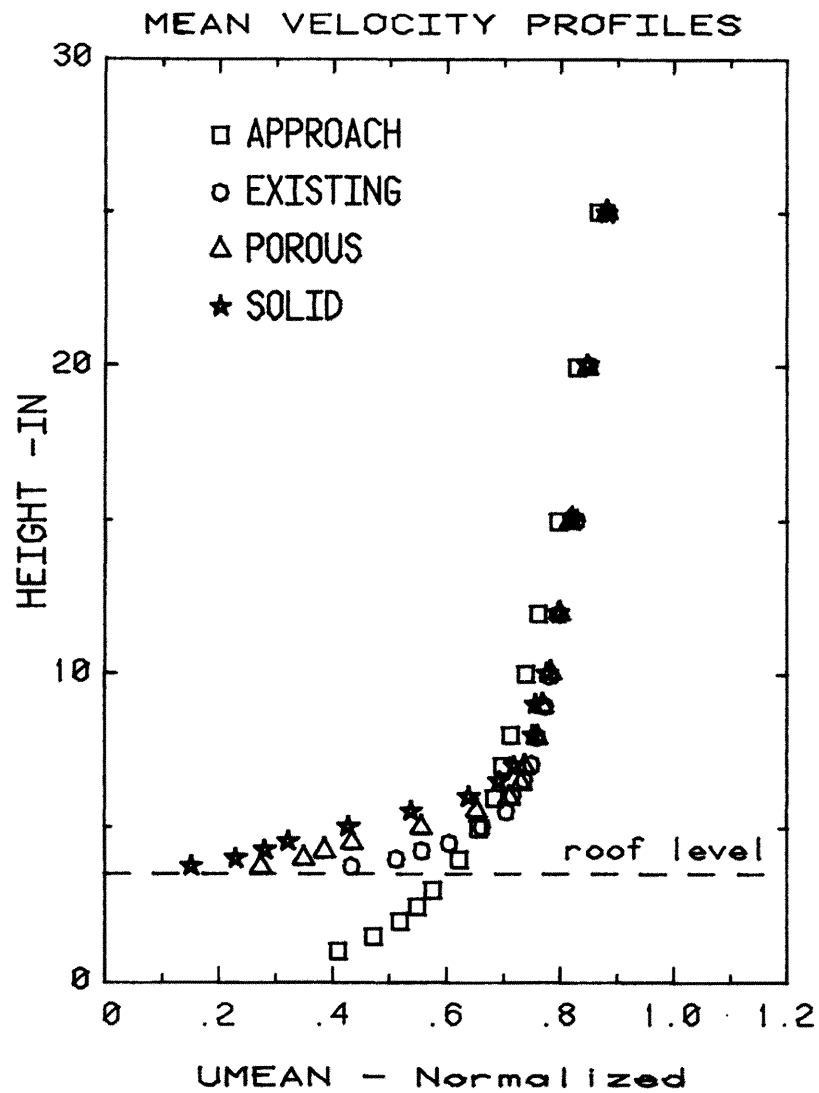


Figure 6a. Mean Velocity and Turbulence Profiles at Measuring Positions

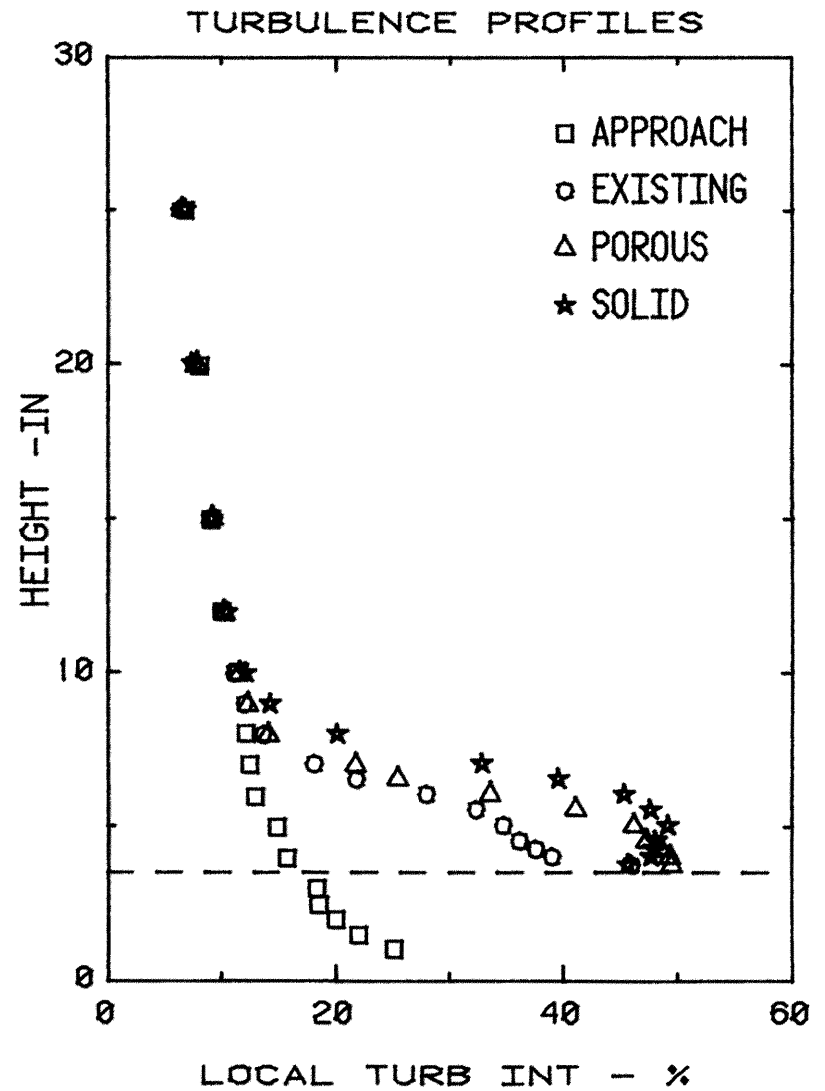
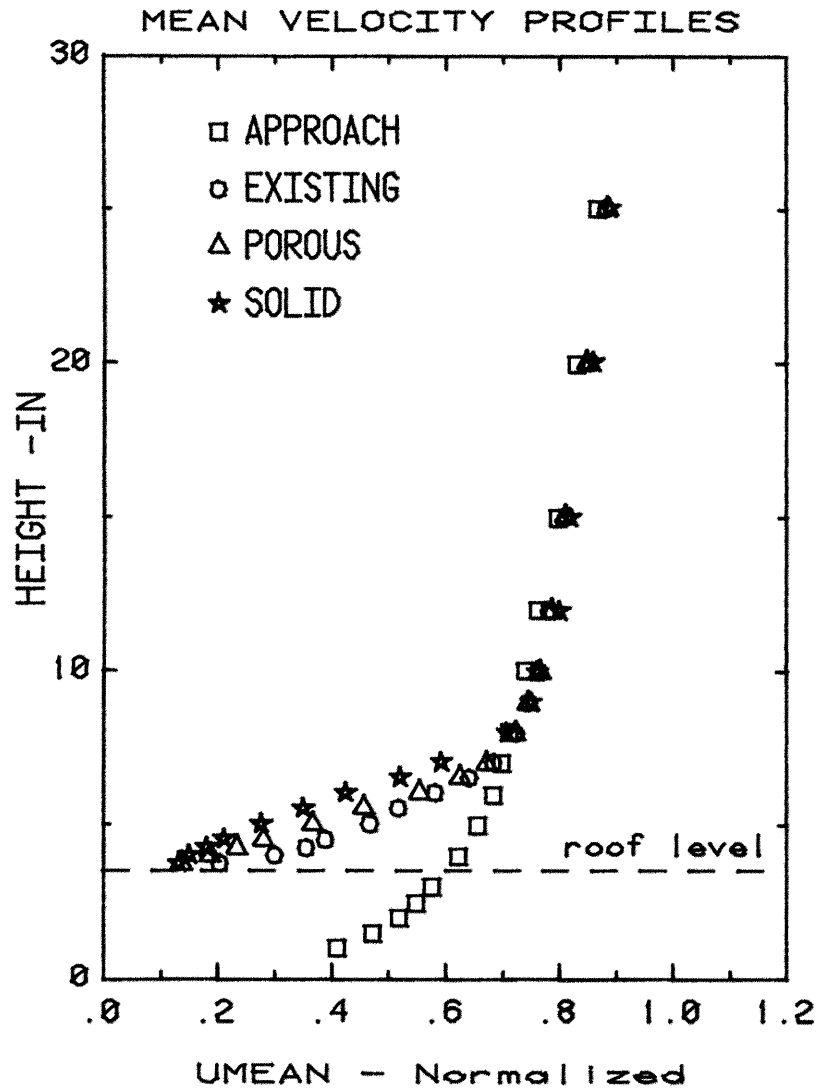


Figure 6b. Mean Velocity and Turbulence Profiles at Measuring Positions

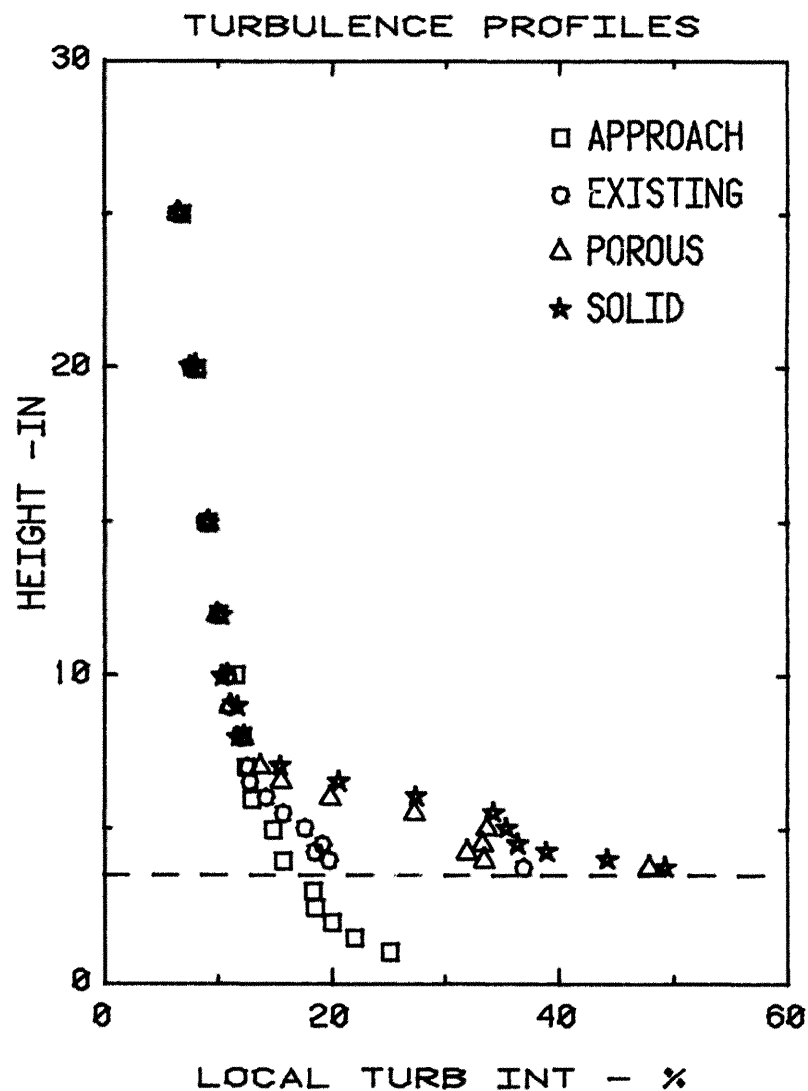
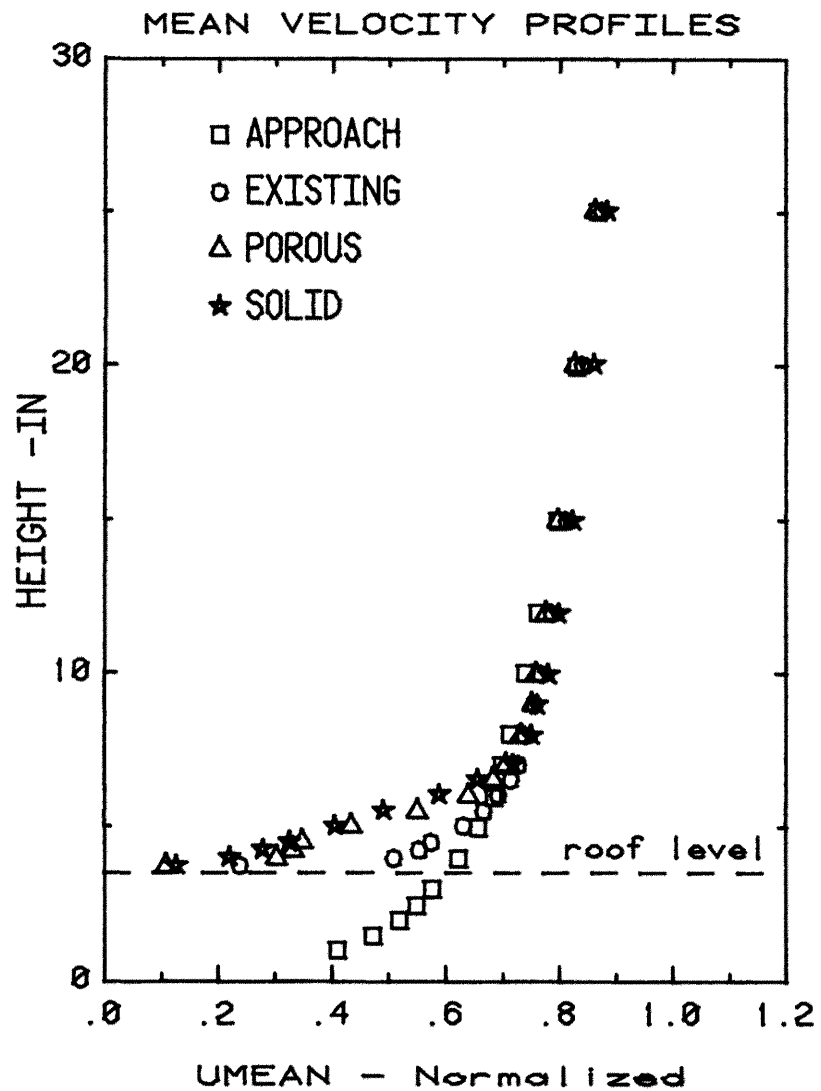


Figure 6c. Mean Velocity and Turbulence Profiles at Measuring Positions

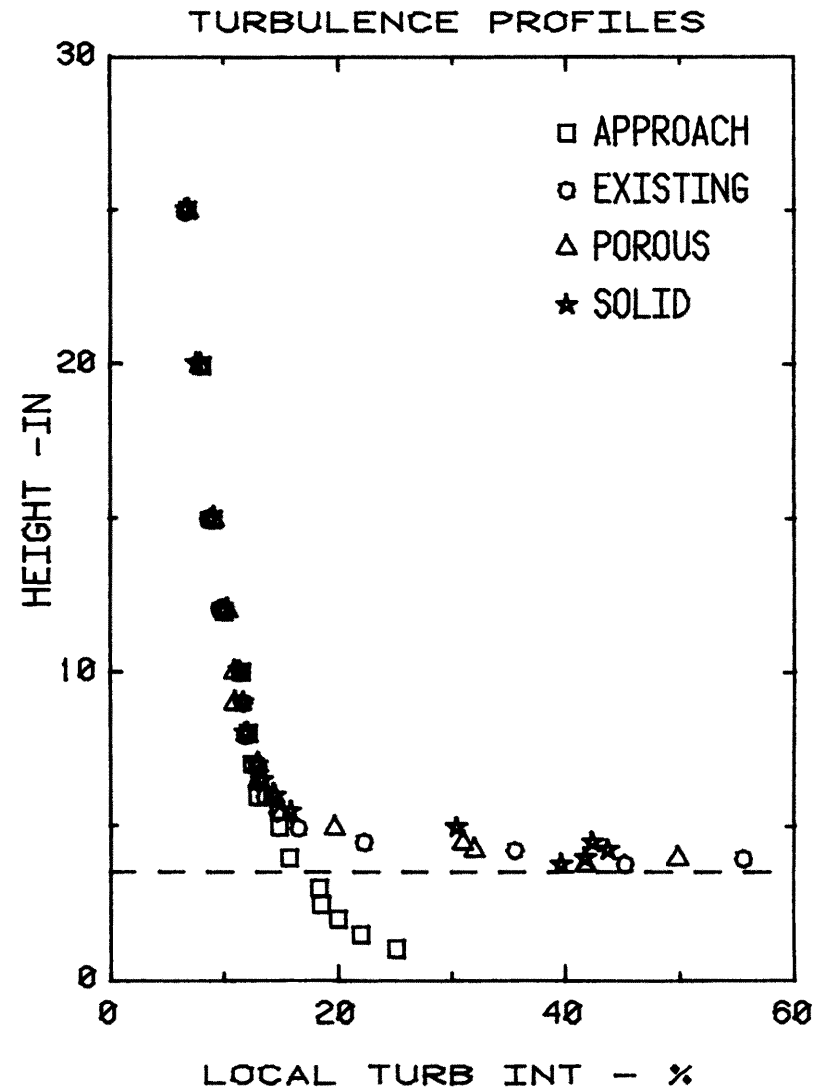
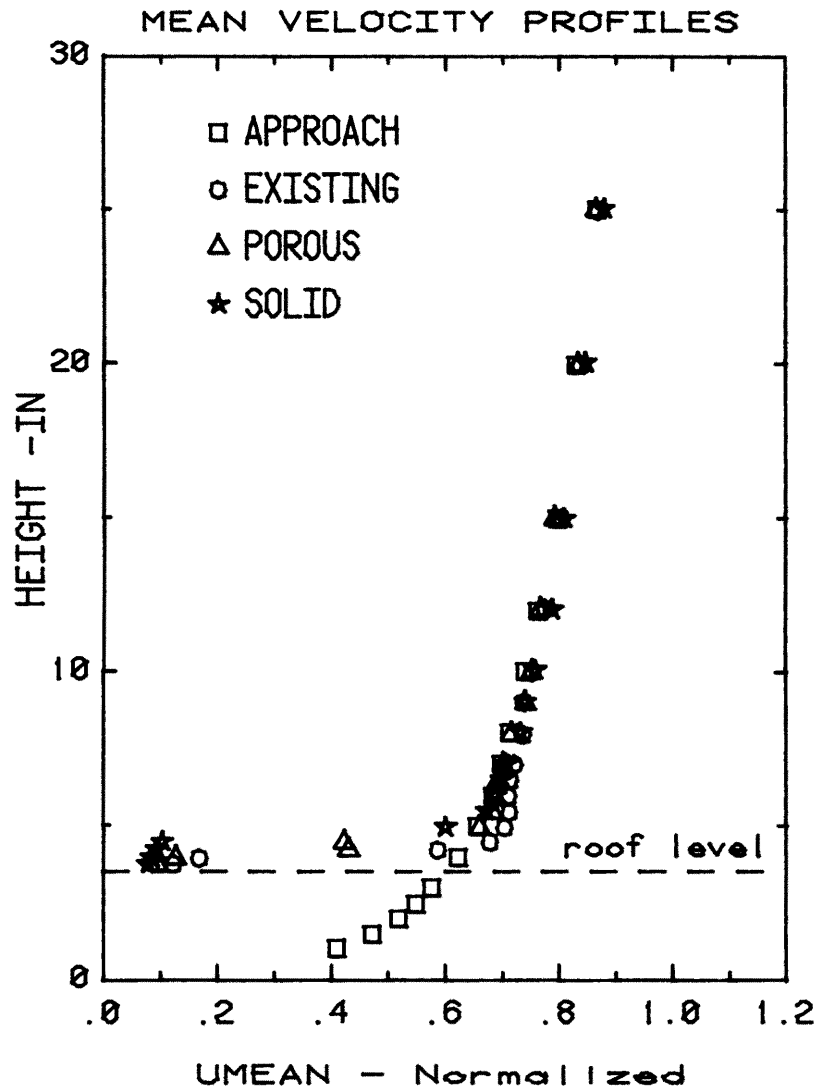


Figure 6d. Mean Velocity and Turbulence Profiles at Measuring Positions

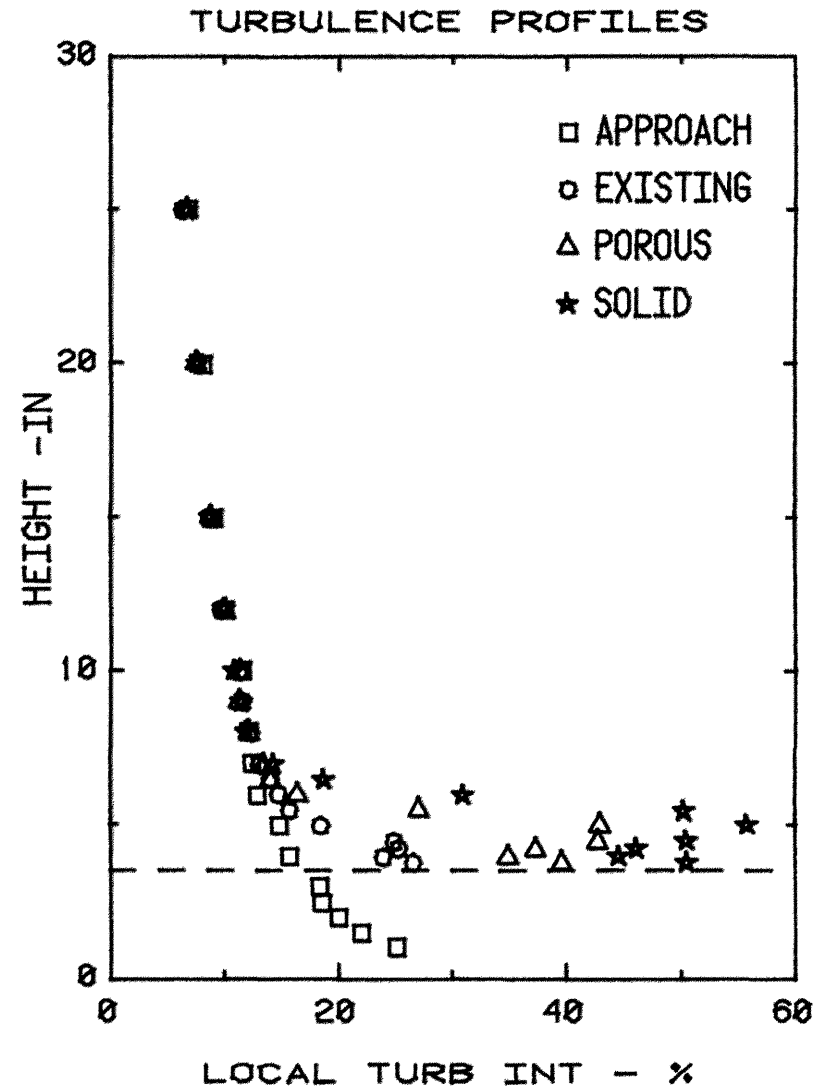
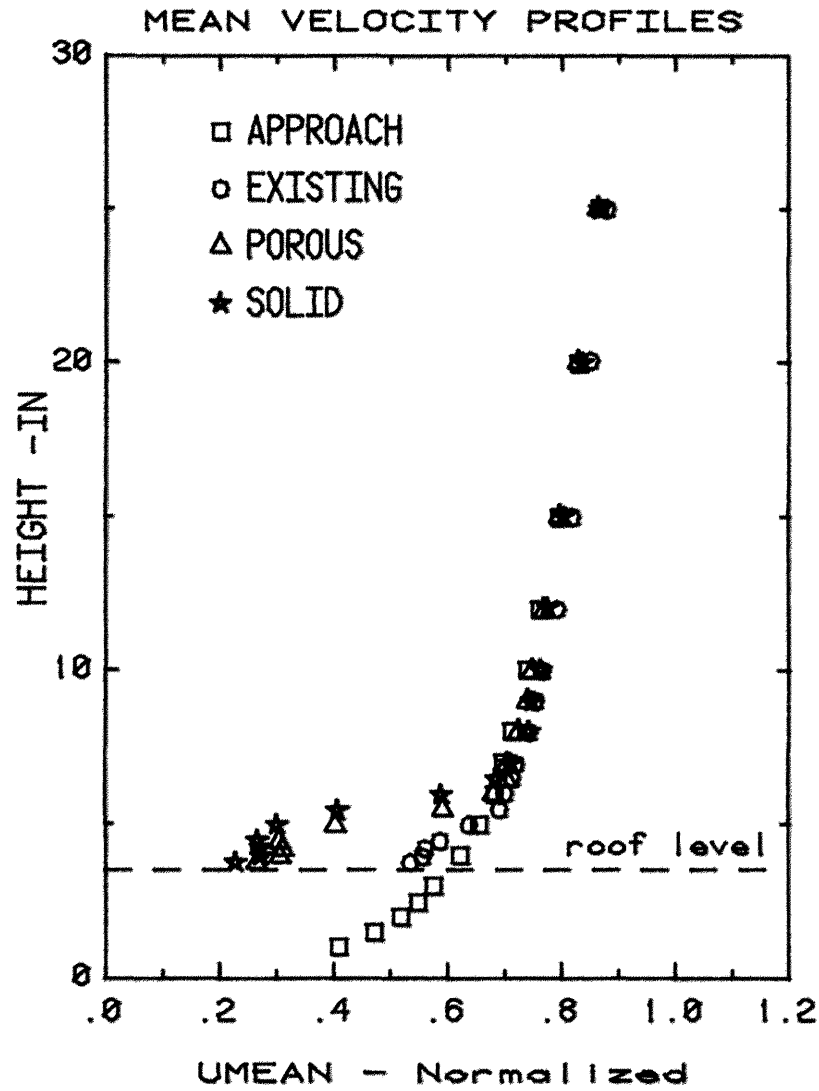


Figure 6e. Mean Velocity and Turbulence Profiles at Measuring Positions

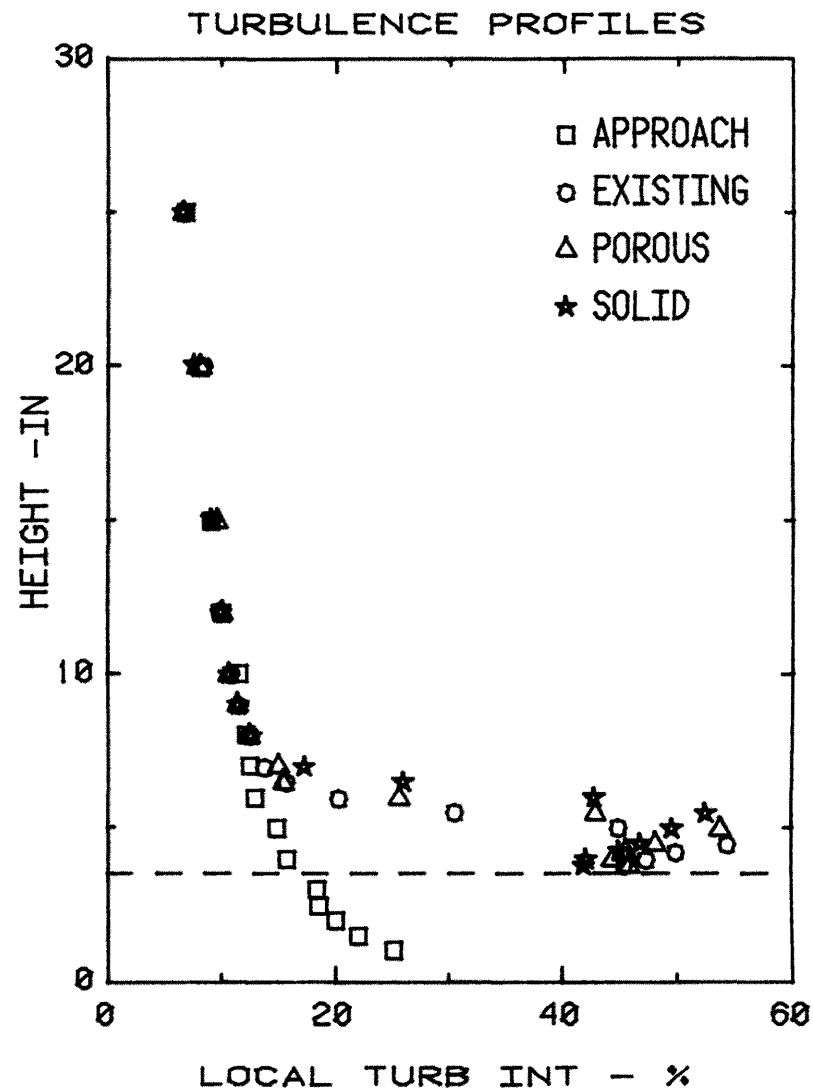
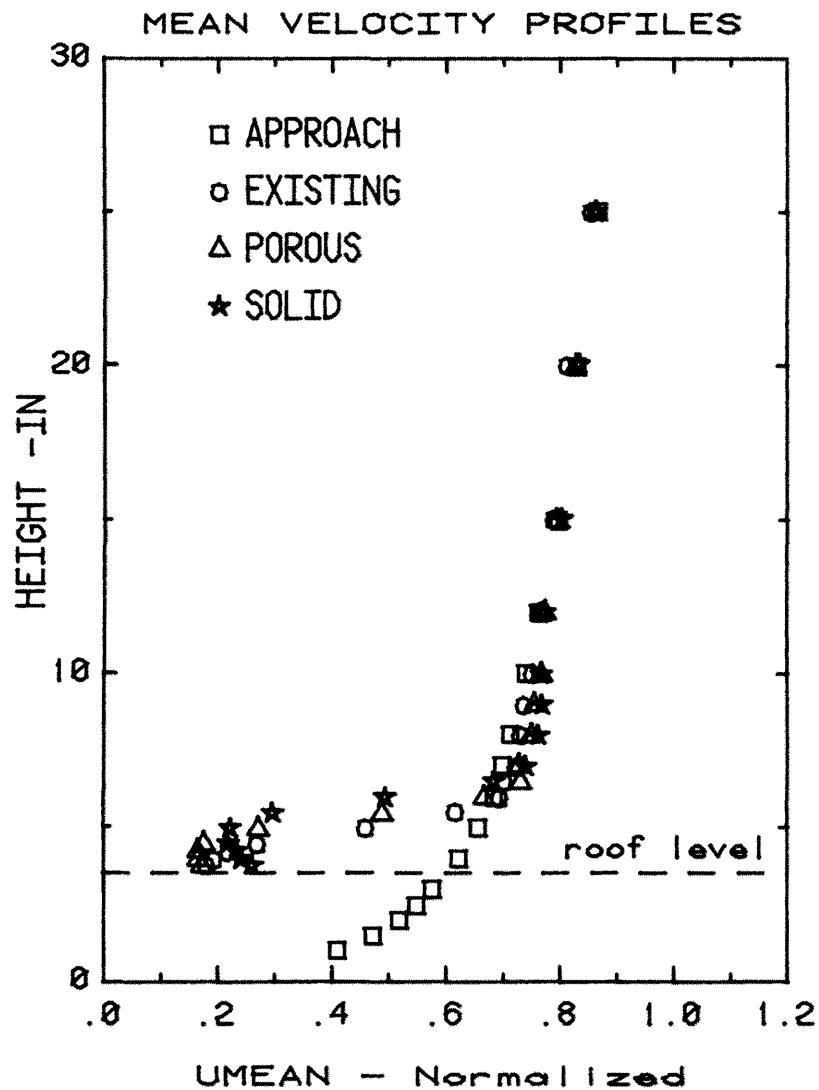


Figure 6f. Mean Velocity and Turbulence Profiles at Measuring Positions

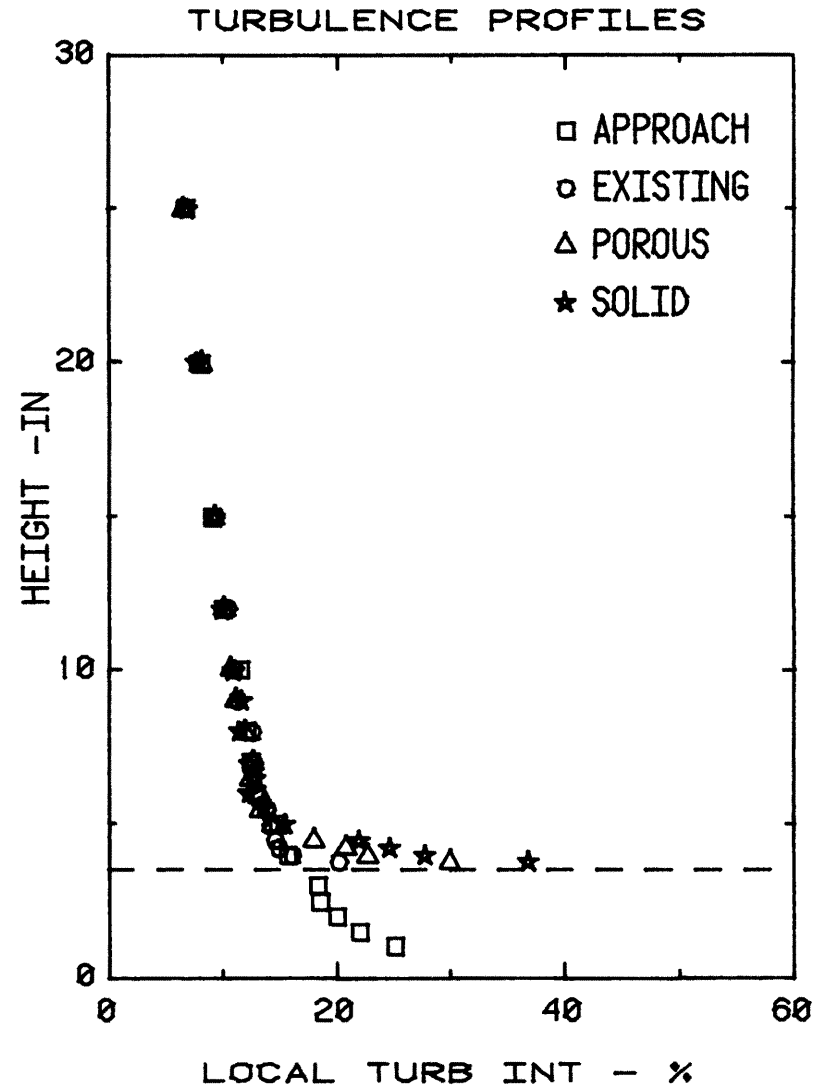
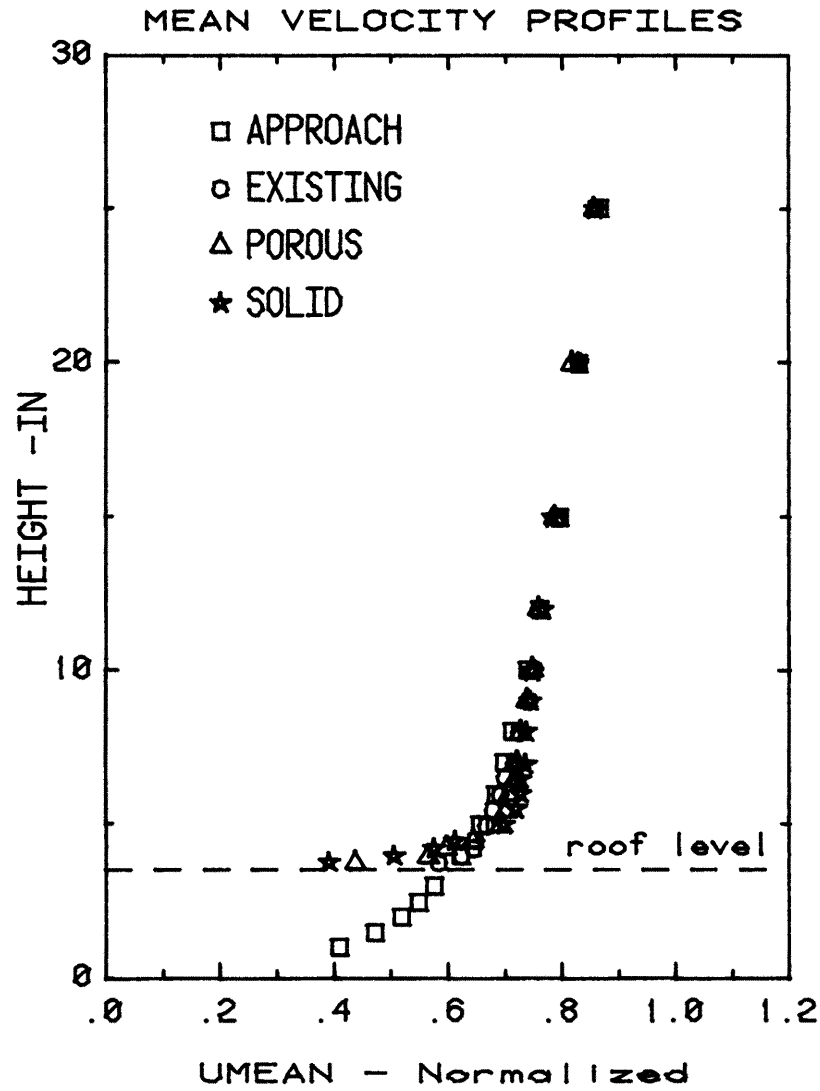


Figure 6g. Mean Velocity and Turbulence Profiles at Measuring Positions

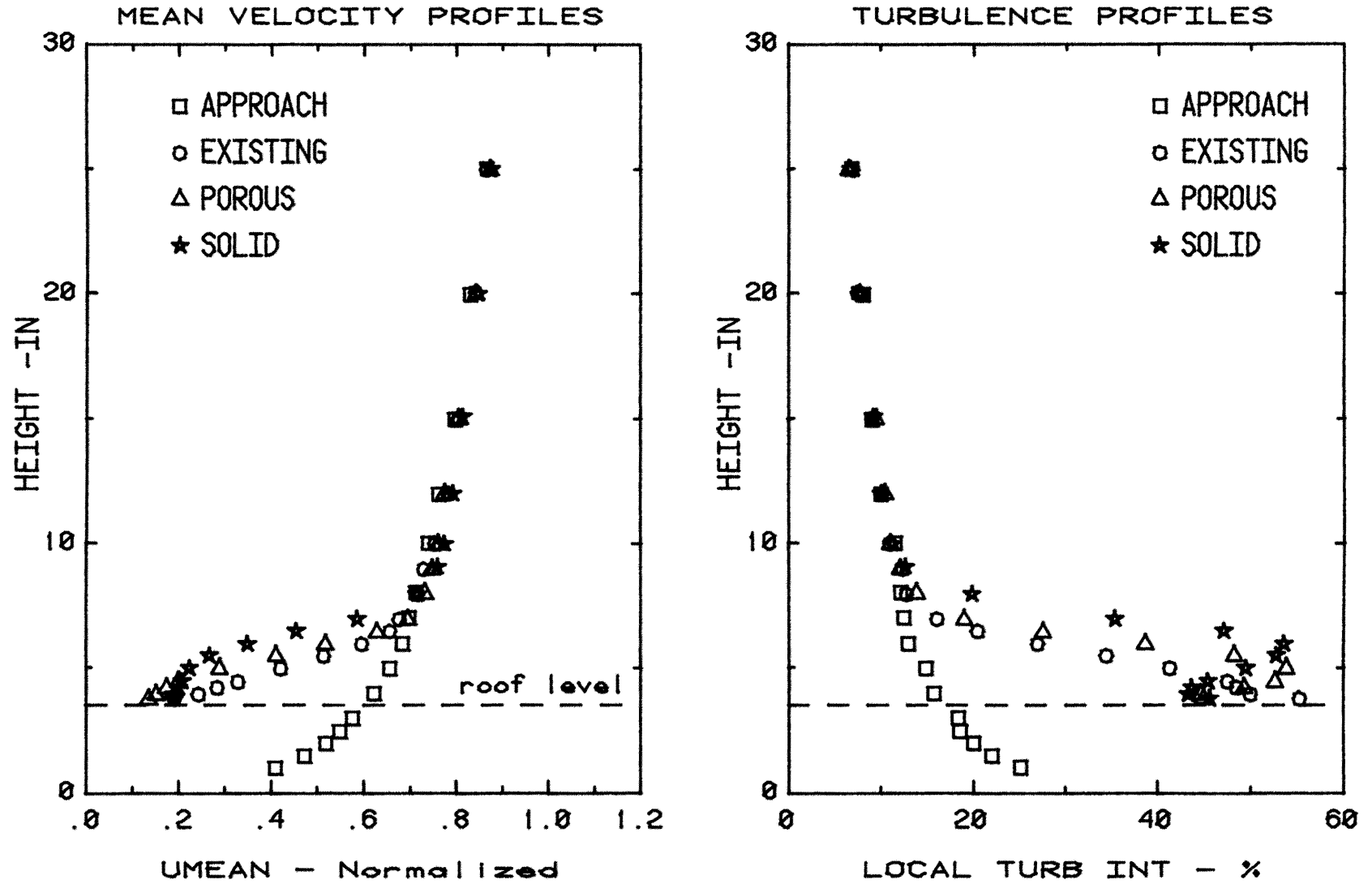


Figure 6h. Mean Velocity and Turbulence Profiles at Measuring Positions

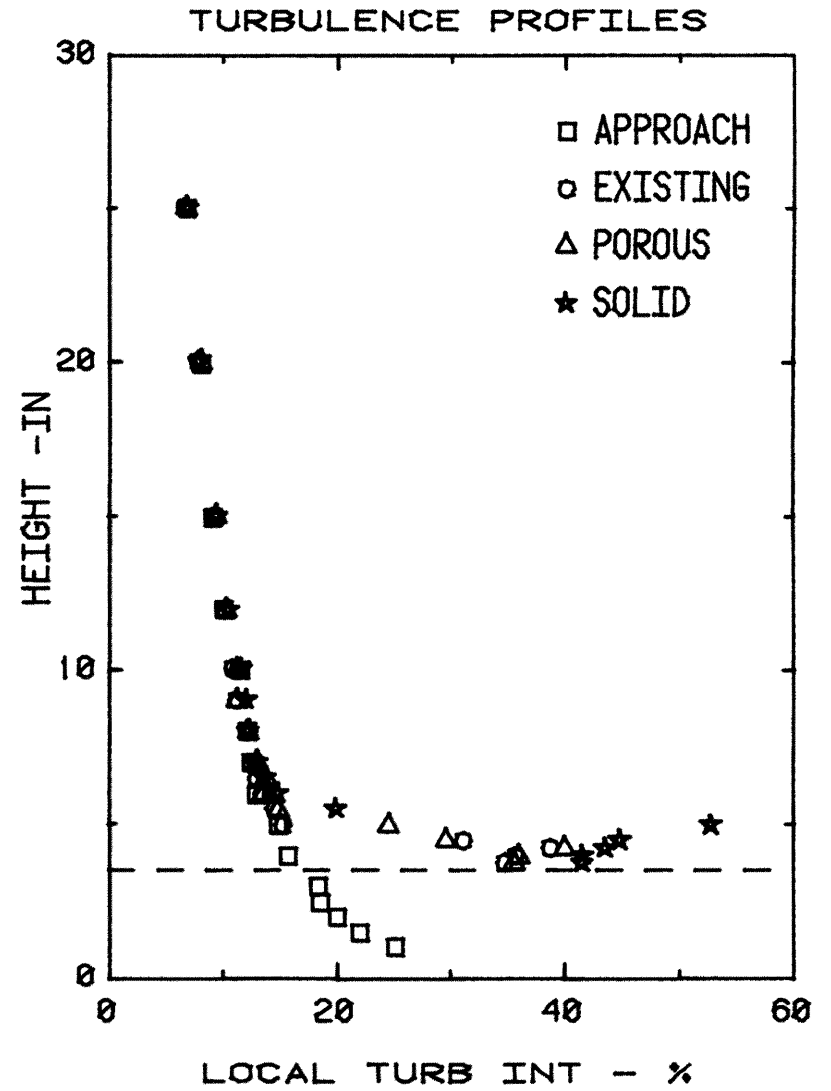
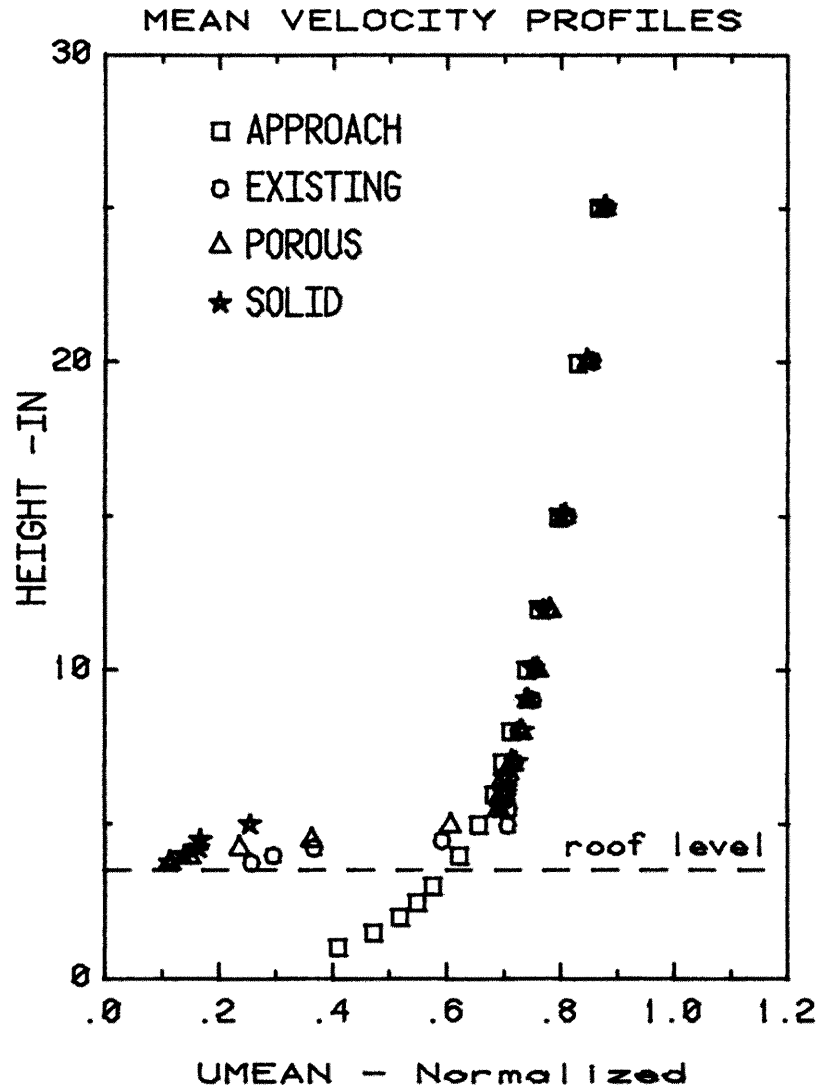


Figure 6i. Mean Velocity and Turbulence Profiles at Measuring Positions

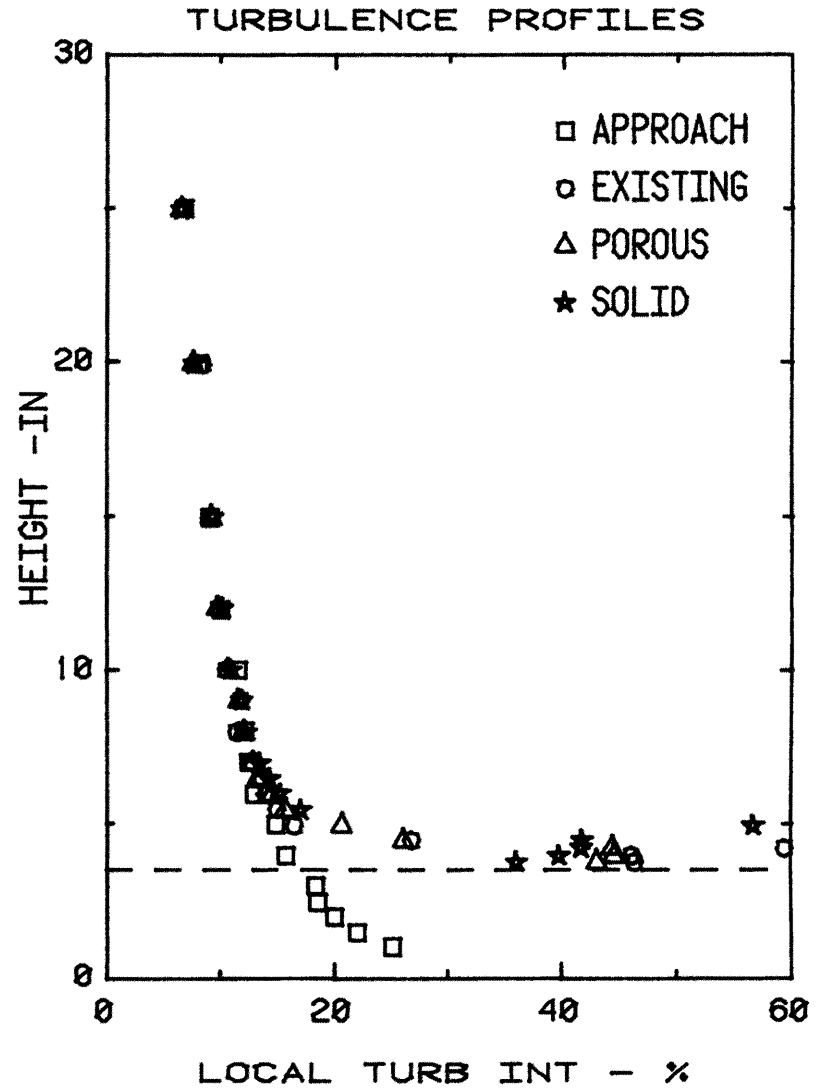
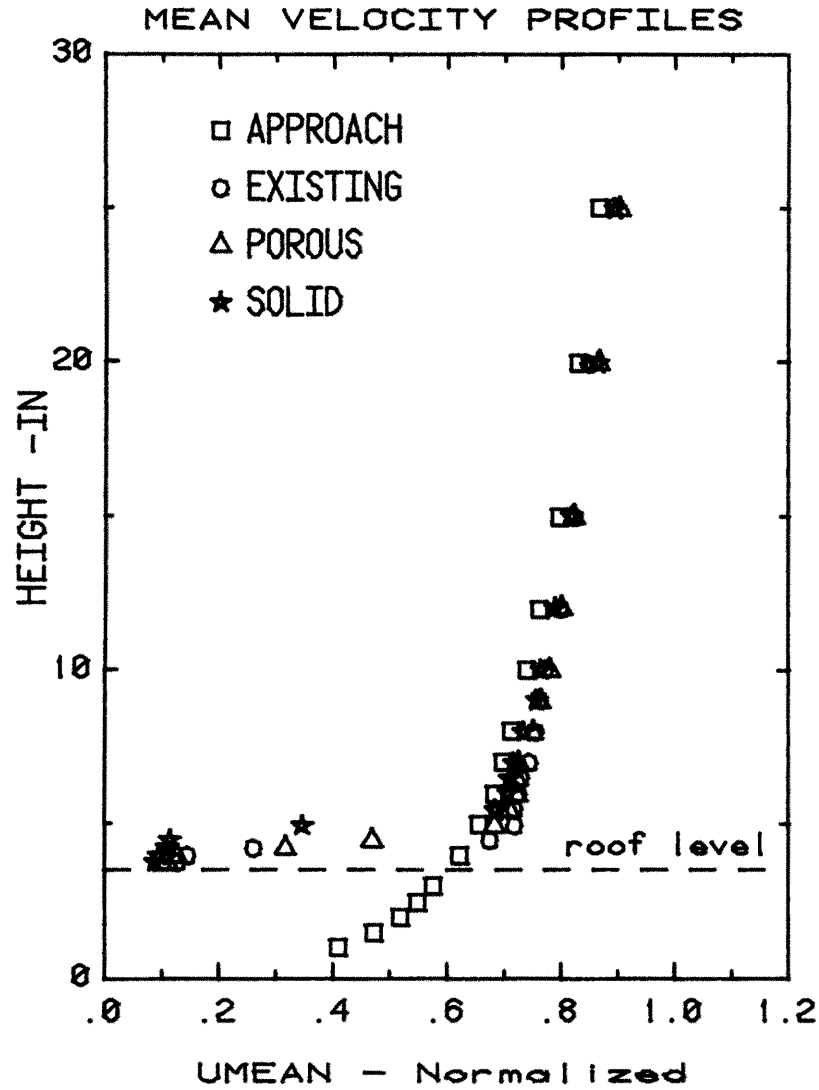


Figure 6j. Mean Velocity and Turbulence Profiles at Measuring Positions

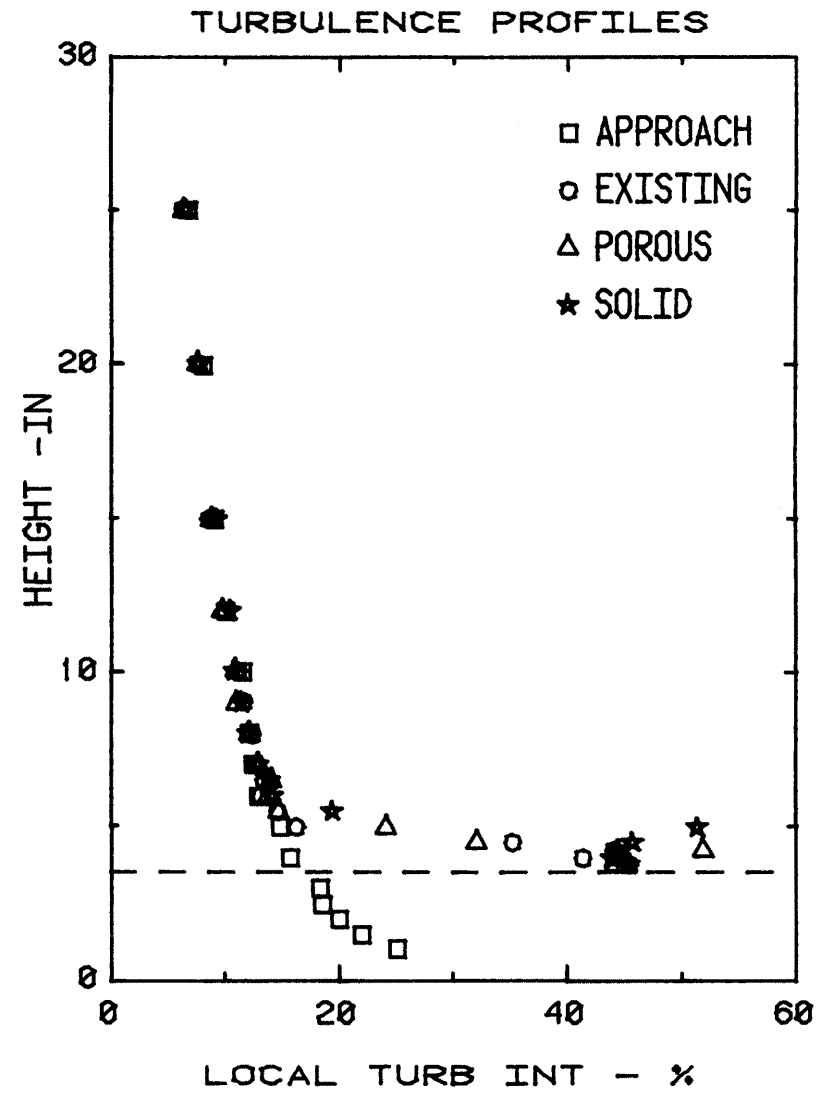
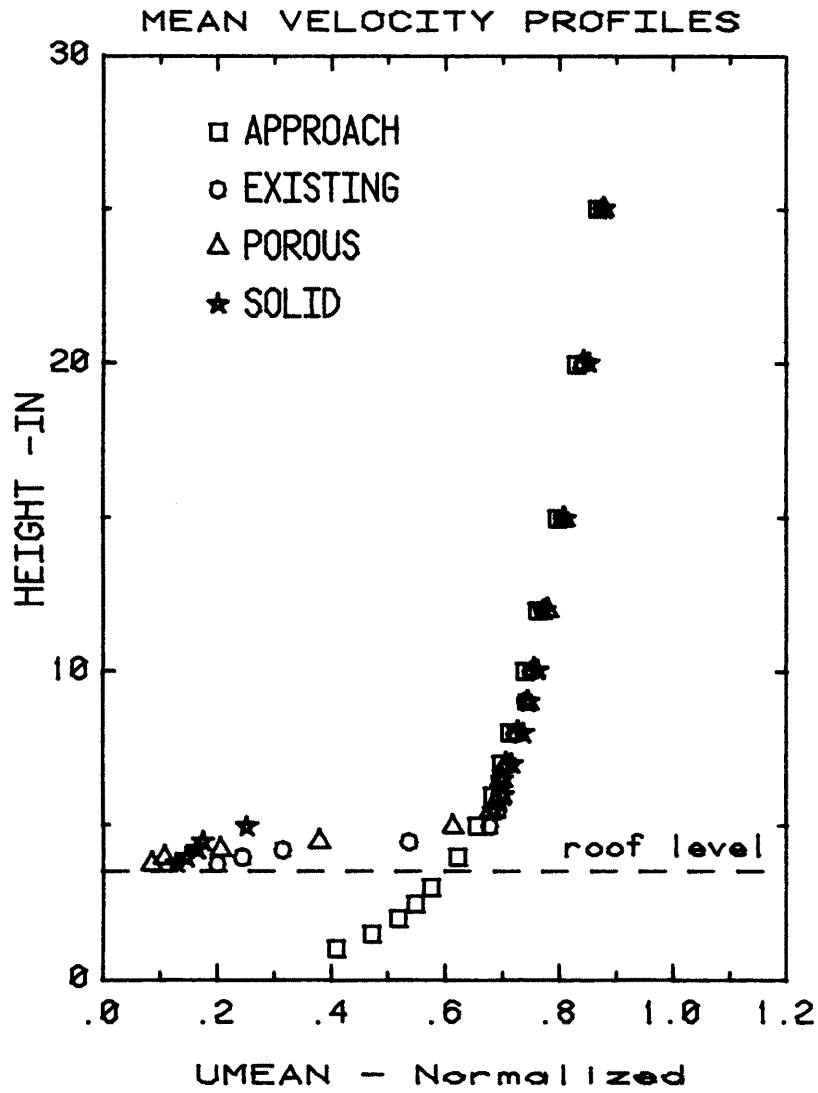


Figure 6k. Mean Velocity and Turbulence Profiles at Measuring Positions

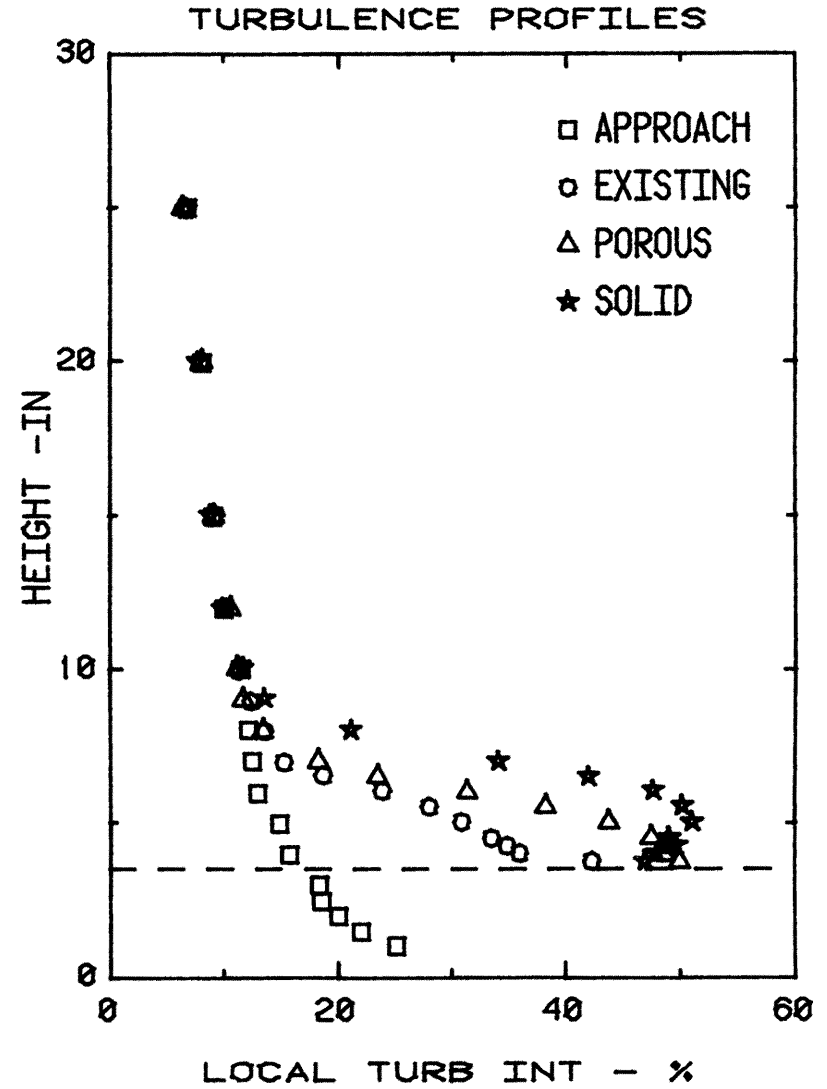
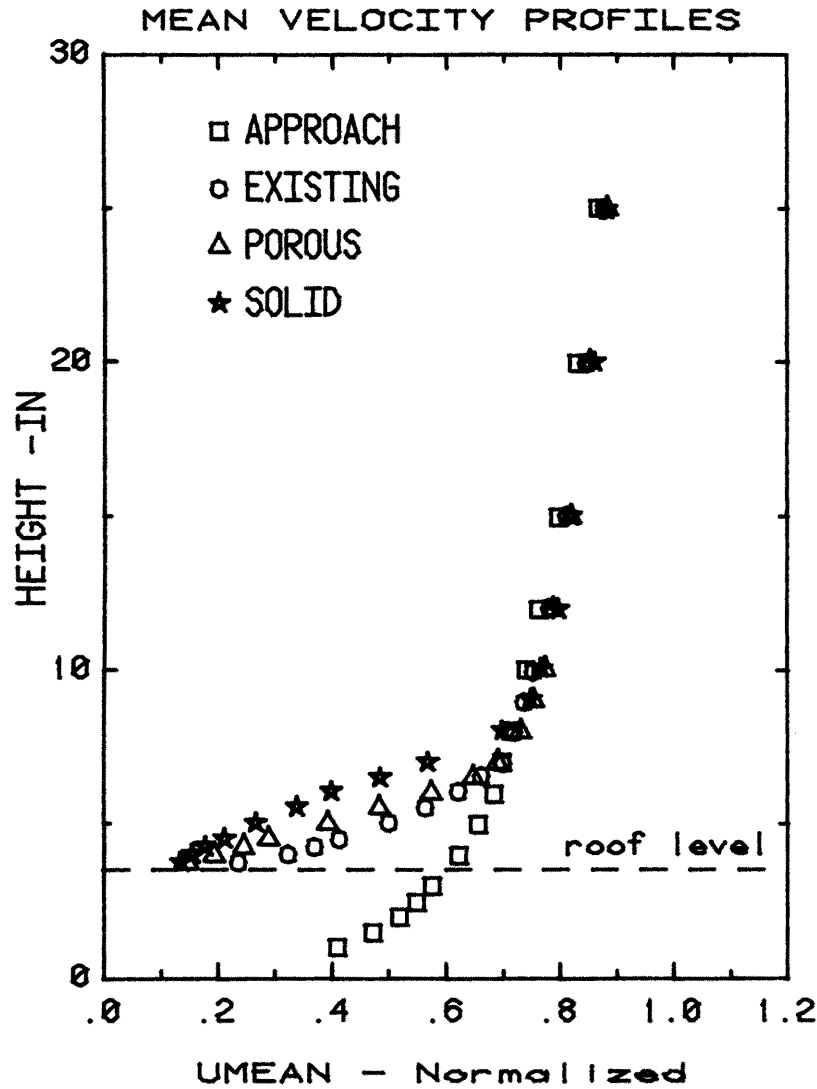


Figure 61. Mean Velocity and Turbulence Profiles at Measuring Positions

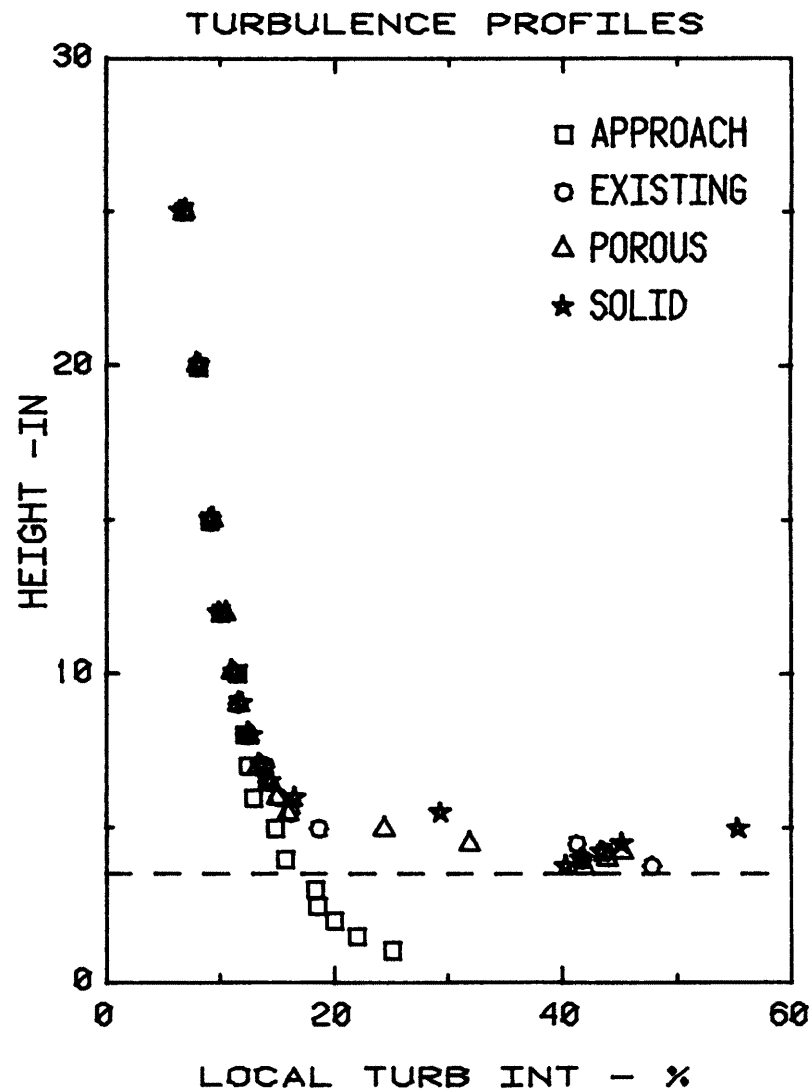
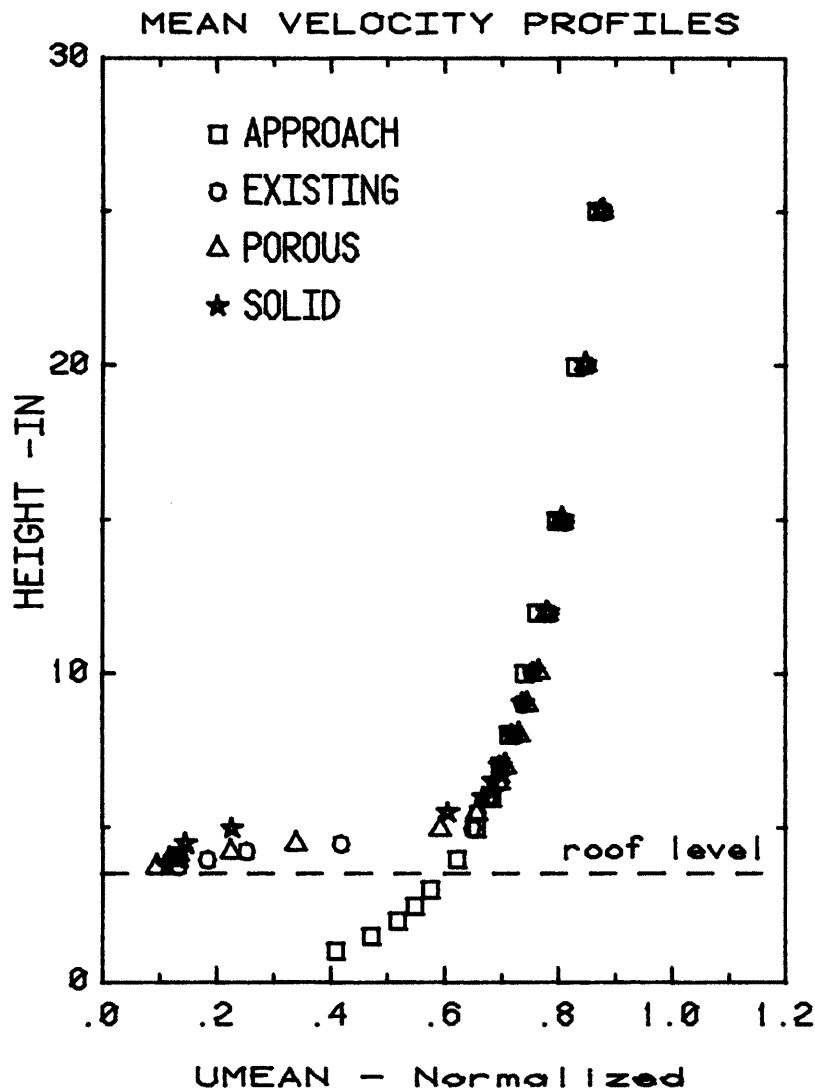


Figure 6m. Mean Velocity and Turbulence Profiles at Measuring Positions

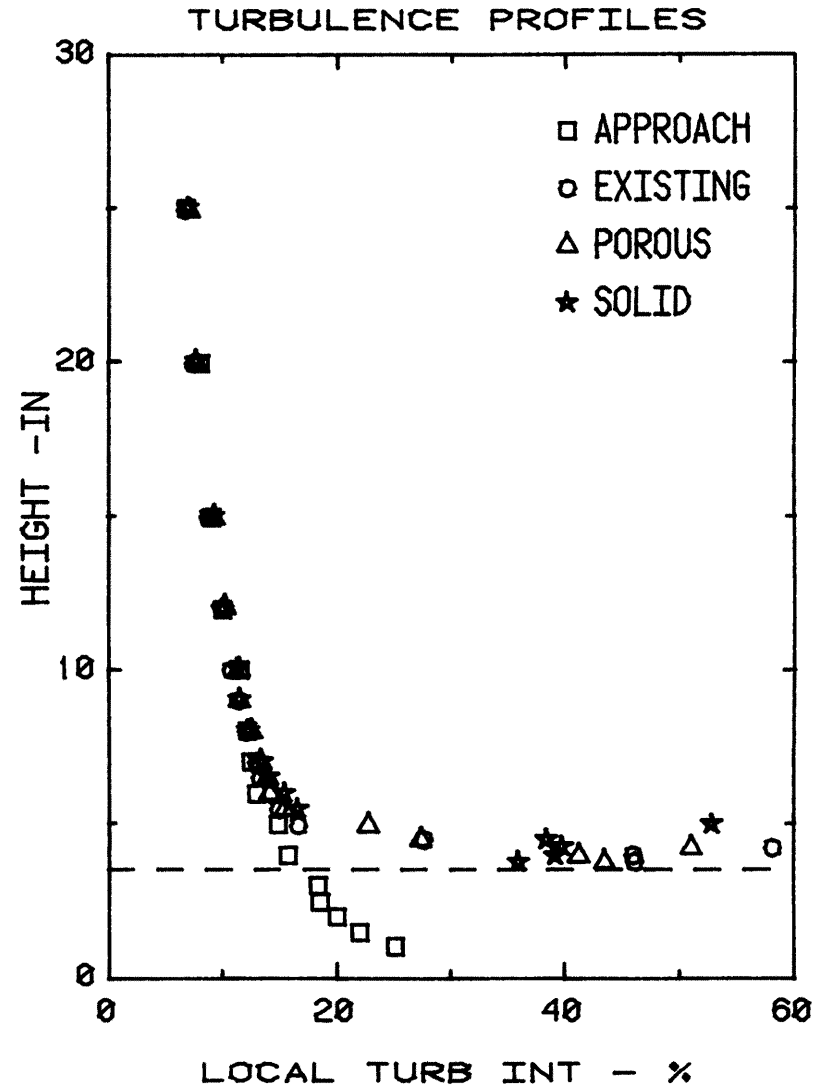
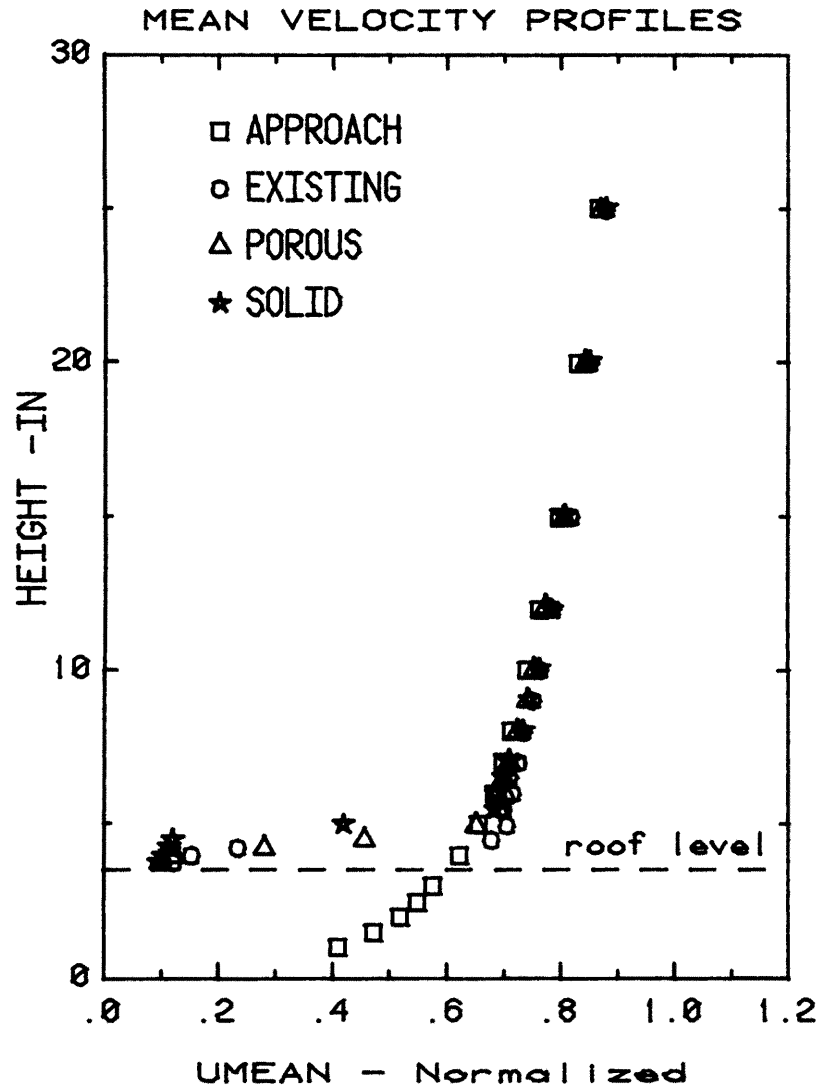


Figure 6n. Mean Velocity and Turbulence Profiles at Measuring Positions

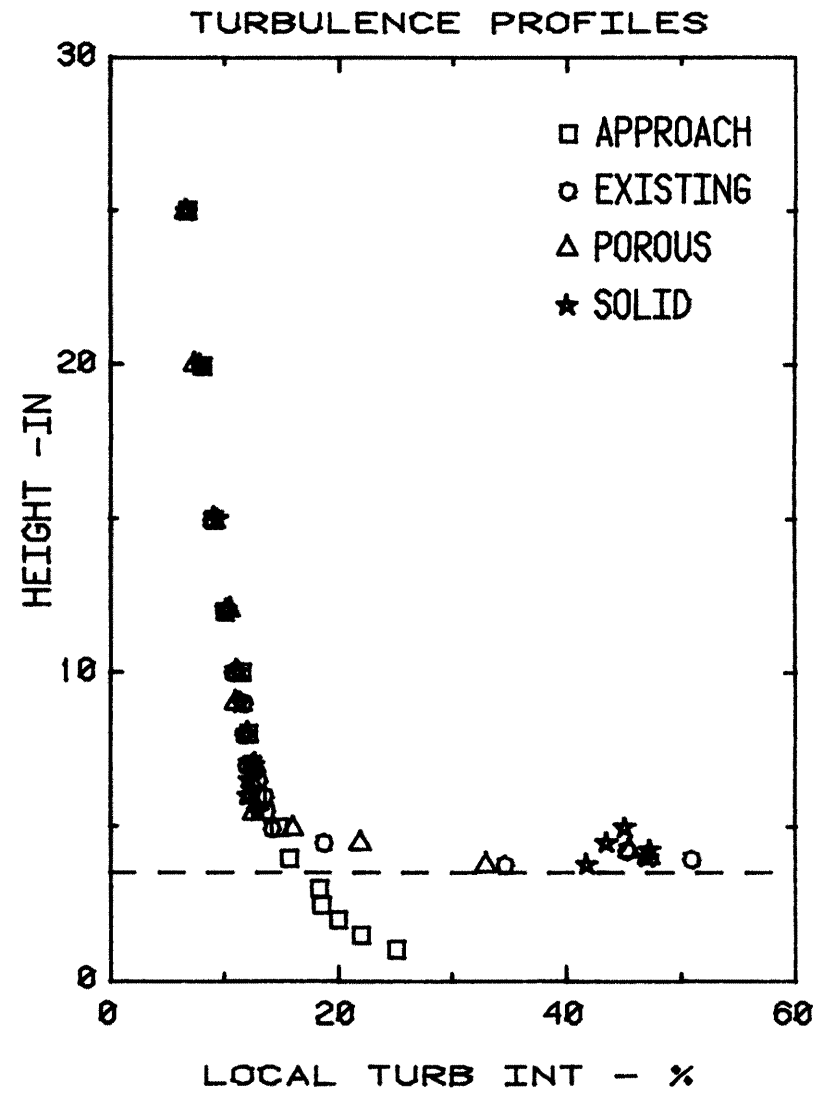
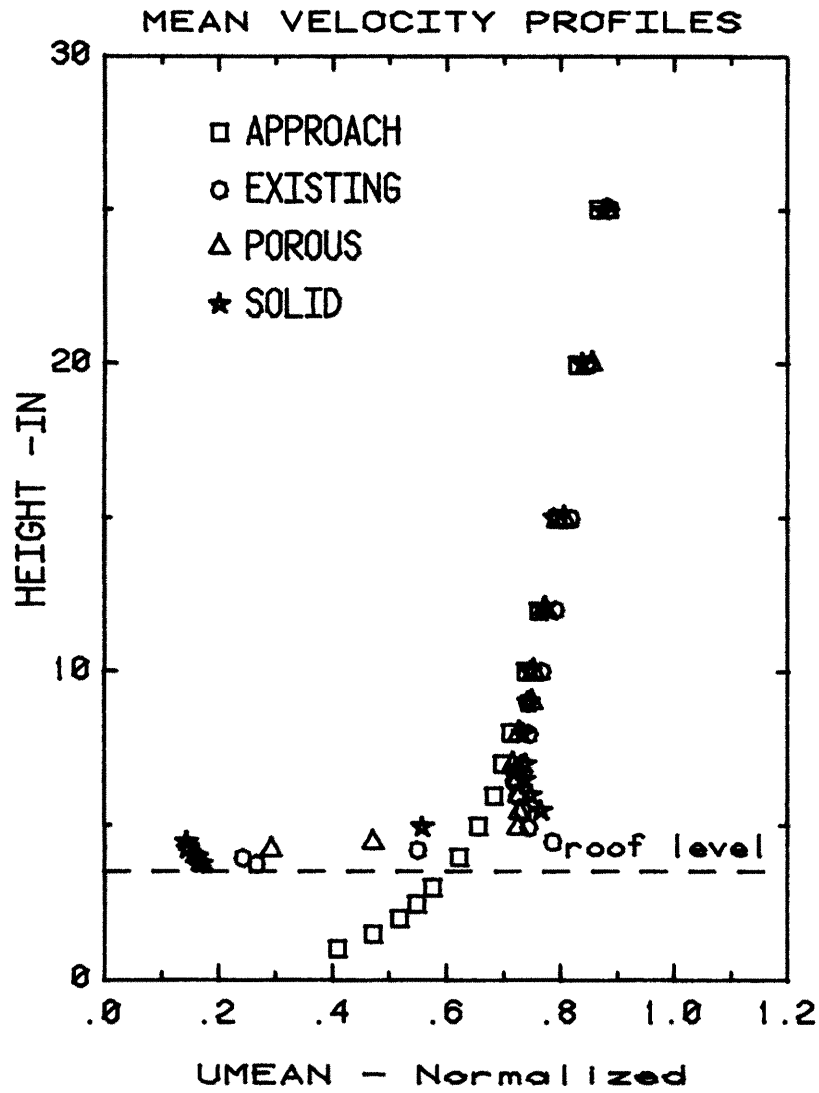


Figure 60. Mean Velocity and Turbulence Profiles at Measuring Positions

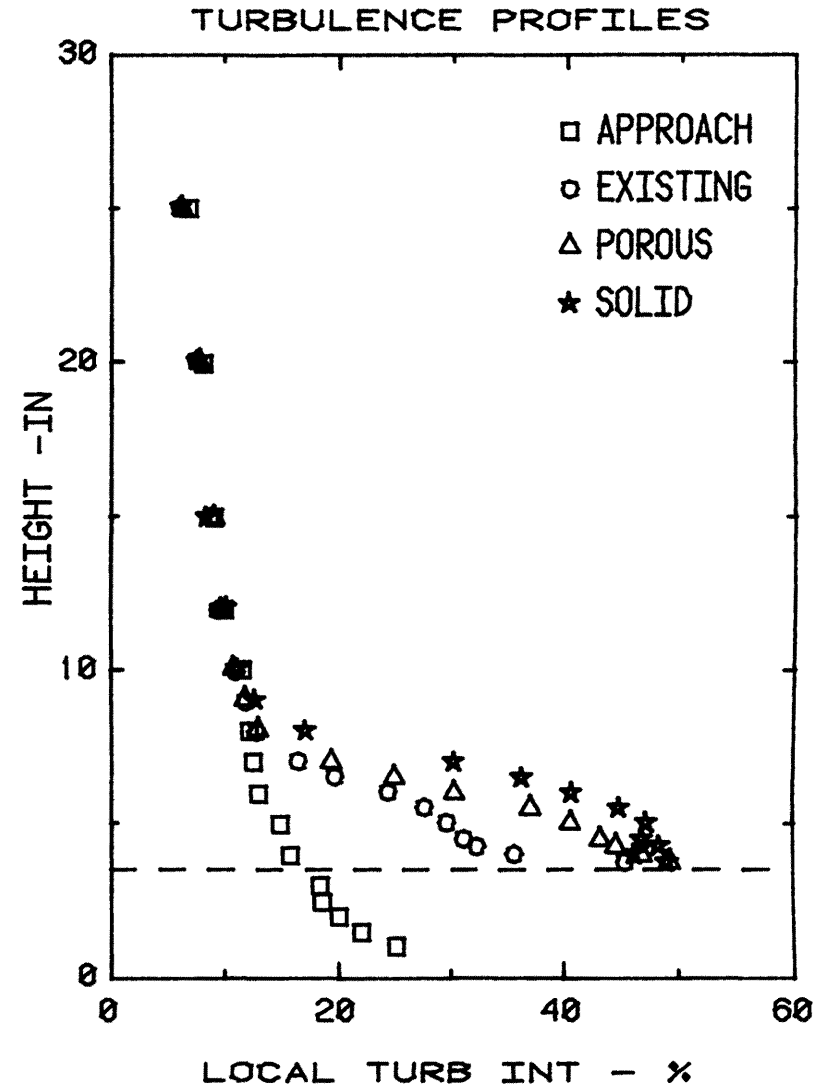
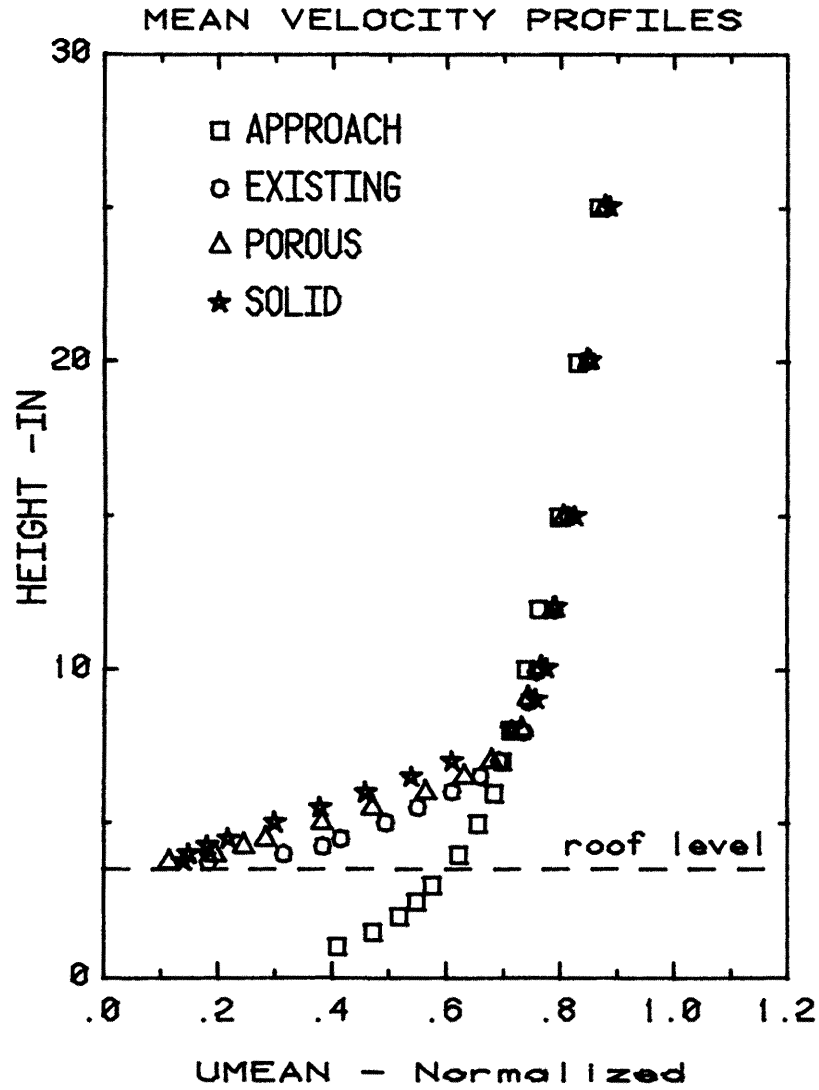


Figure 6p. Mean Velocity and Turbulence Profiles at Measuring Positions

TABLE 1
 FLOW VISUALIZATION GUIDE
 BDM

Configuration A, no heliostats

<u>Run</u>	<u>Azimuth, °</u>
1	45
2	90
3	135
4	270

Configuration A, with heliostats stowed

<u>Run</u>	<u>Azimuth, °</u>
5	45
6	90
7	135
8	270

Configuration A, heliostats active

<u>Run</u>	<u>Azimuth, °</u>
9	45
10	90
11	135
12	270

Configuration B, heliostats stowed

<u>Run</u>	<u>Azimuth, °</u>
13	45
14	90
15	135
16	270

TABLE 1 (Con't)

Configuration B, heliostats active

<u>Run</u>	<u>Azimuth, °</u>
17	45
18	90
19	135
20	270

Configuration C, heliostats stowed

<u>Run</u>	<u>Azimuth, °</u>
21	45
22	90
23	135
24	270

Configuration C, heliostats active

<u>Run</u>	<u>Azimuth, °</u>
25	45
26	90
27	135
28	270